AN INVESTIGATION OF SEVERAL SLOTTED WIND TUNNEL WALL CONFIGURATIONS WITH A HIGH DISC LOADING V/STOL MODEL

T. W. Binion, Jr.

ARO, Inc.

May 1971

Approved for public release; distribution unlimited.

PROPULSION WIND TUNNEL FACILITY
ARNOLD ENGINEERING DEVELOPMENT CENTER
AIR FORCE SYSTEMS COMMAND
ARNOLD AIR FORCE STATION, TENNESSEE

NOTICES

When U. S. Government drawings specifications, or other data are used for any purpose other than a definitely related Government procurement operation, the Government thereby incurs no responsibility nor any obligation whatsoever, and the fact that the Government may have formulated, furnished, or in any way supplied the said drawings, specifications, or other data, is not to be regarded by implication or otherwise, or in any manner licensing the holder or any other person or corporation, or conveying any rights or permission to manufacture, use, or sell any patented invention that may in any way be related thereto.

Qualified users may obtain copies of this report from the Defense Documentation Center.

References to named commercial products in this report are not to be considered in any sense as an endorsement of the product by the United States Air Force or the Government.

AN INVESTIGATION OF SEVERAL SLOTTED WIND TUNNEL WALL CONFIGURATIONS WITH A HIGH DISC LOADING V/STOL MODEL

T. W. Binion, Jr.
ARO, Inc.

FOREWORD

The research reported herein was sponsored by the Arnold Engineering Development Center (AEDC), Air Force Systems Command (AFSC), under Program Element 64719F.

Results of the research were obtained by ARO, Inc. (a subsidiary of Sverdrup & Parcel and Associates, Inc.), contract operator of AEDC, AFSC, Arnold Air Force Station, Tennessee, under Contract F40600-71-C-0002. The research was conducted from July 1, 1966, to June 30, 1970, under ARO Projects No. PD3714, PD3814, PD3914, and PD3014. The manuscript was submitted for publication on March 1, 1971.

The information contained in this report was submitted as a thesis to the University of Tennessee in partial fulfillment of the requirements for a Master of Science degree.

This technical report has been reviewed and is approved.

Charles V. Bennett
Facility Development
Division
Directorate of Civil
Engineering

Ernest F. Moore
Colonel, USAF
Director of Civil
Engineering

ABSTRACT

With the advent of V/STOL model configurations, it became apparent that classical solutions to wind tunnel wall interference problems were not adequate to produce interference-free test results with augmented lift models. The investigation reported herein is the experimental portion of a unified theoretical and experimental search for a slotted wind tunnel wall configuration with minimal interference for conventional and V/STOL models. It is shown that theory and experiment are in excellent agreement for the classical case provided an appropriate expression is used to relate the wall geometry to the boundary condition. Classical data correction equations are not appropriate for the V/STOL case, however. An additional term, not predicted by theory, is needed to account for changes in the jet wake. Geometric parameters which influence the wall interference quantities are indicated. Wall configurations are shown which will produce interference-free force data to a jet-to-free-stream velocity ratio of 4.5. However, additional development work is needed to simultaneously obtain interference-free pitching moment data at velocity ratios greater than two.

CONTENTS

APPENDIXES

I. ILLUSTRATIONS

Figure

NOMENCLATURE

A	Momentum reference area, ft^2
a	Slot width, ft, or polynomial coefficient
C	Tunnel cross-sectional area, ft^2
C_D	Drag coefficient, $D/q_\infty S$
C_{D_f}	Drag coefficient exclusive of direct jet contribution, $D_f/q_\infty S$
C_L	Lift coefficient, $L/q_\infty S$
C_{L_f}	Lift coefficient exclusive of direct jet contribution, $L_f/q_\infty S$

C_m	Pitching moment coefficient, $M/q_\infty S\bar{c}$
$\bar{c}$	Wing chord, ft
D	Drag force, lb
D_f	Drag force exclusive of the direct jet contribution, lb
h	Tunnel semi-height, ft
K	Geometrical slot parameter, ft
L	Lift force, lb
L_f	Lift force exclusive of the direct jet contribution, lb
ℓ	Slot spacing, ft
M	Pitching moment about the wing 1/4-chord, ft-lb
N	Number of points in a set of data
n	Coordinate direction perpendicular to a surface
P	Nondimensional slot parameter, $\left[1 + \frac{K}{h}\right]^{-1}$
q	Dynamic pressure, psf
Re	Reynolds number based on the wing chord
S	Wing planform area, ft^2
U	Stream velocity, ft/sec
u	Streamwise interference velocity, ft/sec
V	Velocity, ft/sec
V_R	Ratio of jet to free-stream velocity
v	Transverse interference velocity, ft/sec
w	Vertical interference velocity, ft/sec
w_o	Momentum theory reference velocity, ft/sec
x	Axial coordinate
x′	Distance between wing and tail, ft
y	Transverse coordinate
z	Vertical coordinate
α	Model angle of attack relative to the free air velocity
α_m	Model angle of attack relative to the tunnel centerline
$\Delta\alpha$	Change in angle of attack due to wall interference
$\Delta\alpha_j$	Jet interference angle, deg

δ	Lift interference factor
λ	Tunnel height-to-width ratio
ρ	Density, slugs/ft^3
τ	Test section porosity, open area divided by peripheral area
τ_w	Wall porosity, open area divided by wall area
ϕ	Perturbation velocity potential

SUBSCRIPTS

$\mathfrak{C}$	Centerline
c	Corrected
H	Horizontal wall
i	Summation index or interference
j	Jet
m	Model
T	Tail
u	Streamwise
V	Vertical wall
W	Wing
w	Upwash or wall
τ	With porous wall
1	First kind
2	Second kind
∞	Free stream

SECTION I
INTRODUCTION

It has long been recognized that wind tunnel walls produce interference effects which significantly affect the data of a lifting airfoil. Two avenues are available to the wind tunnel user to counteract the interference effects: (1) apply theoretical or empirical corrections to the data, or (2) devise a tunnel configuration with negligible interference. Both alternatives have been used with acceptable results in many instances.

However, with the advent of vertical and short takeoff and landing (V/STOL) configurations it became apparent (Refs. 1 and 2) that classical solutions to wind tunnel interference problems were inadequate. Classical theory developed from two basic assumptions:

1. All of the lift is produced by circulation around the wing, and
2. The trailing-vortex-wake flows horizontally downstream.

Both assumptions are inappropriate for a vehicle operating with a large amount of augmented lift. Heyson (Ref. 3) modified the classical theory to consider a nonhorizontal wake. Kirkpatrick (Ref. 4) modified Heyson's wake model by using a distribution of point doublets along short line segments approximating a curved path. The singularity strengths decreased in the downstream direction according to a schedule derived from jets exhausting into free air. While Kirkpatrick's wake representation provided correction factors which were larger than Heyson's, attempts to correct data were in many instances unsatisfactory (Ref. 5, for example).

Because of the lack of satisfactory theoretical correction methods, it has been proposed that to obtain precise data with high lift devices, one should test very small models or use very large wind tunnels. When one considers a V/STOL configuration with six to ten lift engines, the concept of small models is rather impractical, except for very preliminary configuration evaluation. On the other hand, test section sizes for negligible interference approach uneconomical proportions. A third alternative is to devise a test section wall configuration with interferences which are either small enough to be neglected or corrected by analytical means.

The investigation reported herein is the experimental portion of a unified theoretical and experimental search for a wind tunnel wall configuration with minimal interference for V/STOL models. Much of the

theoretical work, by C. F. Lo, has been reported in Refs. 6, 7, 8, and 9. The principal advantages of Lo's results are that solutions can be obtained for arbitrary tunnel cross-sectional shapes and arbitrary peripheral slot distributions. Thus, interference calculations are no longer limited to tunnel configurations which can be represented by the image method.

The primary purpose of this research program was to investigate the wall interference effects associated with augmented lift vehicles. However, it was also desired to obtain information applicable to conventional model configurations. The program has been confined to slotted wall configurations because past experience has indicated that the slotted wall has better characteristics in the low subsonic speed range than porous walls (Ref. 10).

Force and moment data were obtained with a jet-in-fuselage model, balance and sting in the 7 by 10-ft and 15 by 20-ft test sections of the Ling-Temco-Vought (LTV) Low Speed Wind Tunnel. These data, considered essentially interference free, were used to evaluate wall interference by comparison with data obtained with various wall configurations in the 30 by 45-in. test section of the Arnold Engineering Development Center Low Speed Wind Tunnel (V/STOL).

While the LTV tests were conducted with the jet-to-free-stream velocity ratios from 0 to 30, the tests in the V/STOL tunnel have been limited to a velocity ratio of 4.5. The limitation is due to the "flow breakdown" problem identified in Ref. 11. It has been shown (Refs. 11 and 12) that flow breakdown is caused by the model wake interacting with the tunnel floor producing a flow field which deviates substantially from that experienced in free flight. Thus, particularly in a closed test section, there is a maximum velocity ratio above which the data are not valid.

Approximate wake paths are shown in Fig. 1 (Appendix I) for the model installation used herein. The paths were computed from an empirical formula developed in Ref. 13. It may be seen that, at a velocity ratio of 4.5 and high angles of attack, the jet impinges nearly normal to the floor. At approximately a velocity ratio of 5.0, the jet flow turns forward, causing a large vortex to form ahead of the model, thereby severely distorting the uniform stream. Thus, the velocity ratio of the tests was limited to avoid an additional complication to the problem.

SECTION II
APPARATUS

2.1 WIND TUNNELS

The data which are considered interference free were obtained in the Ling-Temco-Vought (LTV) Low Speed Wind Tunnel. The LTV tunnel is a horizontal, continuous-flow, atmospheric pressure, single-return, closed throat system. The rectangular 15 by 20-ft test section is followed by a 7 by 10-ft test section with speed ranges from 12 to 60 ft/sec and 80 to 320 ft/sec, respectively. A complete description of the tunnel, its operating characteristics and associated equipment, is contained in Ref. 14.

The wall interference study was conducted in the Arnold Engineering Development Center (AEDC) Low Speed Wind Tunnel (V/STOL). The V/STOL tunnel is a continuous-flow, closed-circuit, atmospheric pressure test unit in which speeds from 5 to 220 ft/sec can be attained. The test section has a 30- by 45-in. cross section and is 72 in. long. The horizontal test section walls are mounted on a variable number of support columns which allow a wide variety of wall configurations to be used. The vertical wall liners are supported on a web framework and were solid for most of the investigation. The test section is enclosed in a sealed plenum which allows a constant-pressure field equal to the free-stream static pressure to be maintained around the test section. A complete description of the V/STOL tunnel, its operating characteristics and associated equipment, is presented in Ref. 15.

2.2 MODEL

The jet-in-fuselage model, shown installed in the V/STOL Tunnel in Fig. 2, consists of an air ejector surrounded by a minimum cross-sectional area fuselage, a midfuselage wing, and a removable horizontal tail. The pertinent model dimensions are given in Fig. 3.

The air ejector and its inlet were mechanically separated from the fuselage. The flow resistance through the 0.01-in. gap between the ejector and fuselage was increased by using a labyrinth seal. The ejector has an inlet diameter of 3.25 in. and an exit diameter of 2.6 in. and is capable of generating 85 lb of thrust. The ejector exit is coincident with the bottom of the fuselage. High-pressure nitrogen was supplied to the ejector through a specially designed sting. A description of the ejector and its operating characteristics may be found in Ref. 16.

The fuselage has a square cross section with the corners rounded with a 0.25-in. radius. The model has a rectangular planform wing whose 1/4-chord line intersects the ejector centerline. The wing has a NACA 0012 airfoil section and is at 0-deg angle of attack with respect to the fuselage. The horizontal tail also has a NACA 0012 airfoil section and is also at zero incidence to the fuselage.

The model contains two strain-gage balances. One measures the normal force of the ejector and its inlet. The other measures the normal force, axial force, and pitching moment of the wing-fuselage-tail assembly. The model was mounted in the V/STOL tunnel so that the pitch center coincided with the wing 1/4-chord line.

2.3 WALL CONFIGURATIONS

Data were obtained with seven basic wall configurations. A letter (A through G) is used to denote a particular configuration class and is synonymous with a slot shape characteristic of that class. Unless otherwise stated, each configuration consisted of solid vertical walls and ten slots in each horizontal wall. Each wall was constructed from individually supported 1/4-in.-thick plates whose edges were machined to produce a given slot configuration. Porosity variations were accomplished by removing the plates from the tunnel and machining the edges so that the width of a slot or slots was increased as indicated in the description of the individual configurations.

The configurations may be divided into two groups. Configurations A to D had slot centerlines located such that there was a slat directly above and below the tunnel centerline; whereas, Configurations E to G had a slot on the tunnel centerline, thereby resulting in a half-slot at each side of the wall. The slot shapes and their relation to the model are shown in Fig. 4.

Configuration A: The theoretical formulations assume a constant width slot extending from infinity to infinity in the streamwise direction. Configuration A approximates the theoretical configuration with constant width slots (Fig. 4a) extending the length of the test section. The Configuration A slot shape was also used to form a test section configuration with seven slots in each vertical wall and solid horizontal walls in addition to the most general test section arrangement described above. Porosity variations were accomplished by increasing the slot width.

Configuration B: The Configuration B slot has a constant width from the beginning of the test section to Station 36. The slot width then

decreased linearly to zero at the end of the test section. Porosity was changed by increasing the maximum slot width.

Configuration C: The slot width varied linearly from zero at the beginning to a maximum at the end of the test section. Porosity variations were made by changing the maximum slot width.

Configuration D: The slot for Configuration D and all subsequent configurations began at Station 20. The slot tapered linearly to Station 36, had a constant width to Station 60, and then tapered to zero width at Station 72. The slot shape was derived from theoretical solutions for the axial distribution of lift interference (Ref. 8) which indicate that zero upwash interference may be attained along the tunnel centerline by varying the slot width with axial position. The theoretical slot width variation to obtain zero lift interference in the V/STOL tunnel with ten slots in each horizontal wall for a velocity ratio of approximately 3.2 is shown in Fig. 5. Also shown is the slot shape for Configuration D which was selected to approximate the theoretical shape. Porosity was varied by changing the value of the maximum slot width.

Configuration E: The slot shape and location with respect to the model were the same as Configuration D, except the rear taper was eliminated and the slat centerlines were shifted to obtain a slot on the tunnel centerline (Fig. 4b). The maximum width of each slot was increased uniformly until the data obtained at zero velocity ratio indicated zero upwash interference which occurred with τ = 2.14 percent. Thereafter, porosity variations were accomplished by varying only the width of the center slots; that is, the slots directly above and below the model.

Configuration F: Configuration F is similar to Configuration E in that all slots except the center slot had the shape of Configuration E with the maximum slot width (0.263 in.) established by producing the correct lift at zero velocity ratio. The center slot had a shape as shown in Fig. 4b. Only the width of the rectangular area directly above and below the model was opened to achieve a porosity variation. The length and position of the opened rectangle correspond to the jet impingement region for V_R of 3.3 and 4.5 shown in Fig. 1.

Configuration G: Near the end of the experimental program, theoretical calculations (Ref. 9) indicated that a test section configuration with solid vertical walls, a small porosity on the top wall, and a moderate porosity on the bottom wall would produce zero upwash interference independent of the velocity ratio. Configuration G was devised by using an existing top wall with τ_w = 3.6 percent with a slot shape the same as

Configuration E. The bottom wall configuration began by using the Configuration E slot shape with τ_w = 19.3 percent, giving an overall porosity of 6 percent. Subsequent changes were then made by changing only the rear portion of the bottom wall. The resulting slot shape (Fig. 4b), tapered from Station 20 to Station 36, had a constant width (1.5 in.) to Station 44, tapered linearly again to Station 50 and had a second constant width section to Station 72. Only the width of the second constant width section was increased to increase porosity.

2.4 INSTRUMENTATION

The ejector thrust and the model normal force, axial force, and pitching moment were obtained from strain-gages placed on specially designed balance beams. The tunnel nozzle-exit pressure, which was used as a reference for all other pressure measurements, was measured with a precision mercury manometer. The ejector-exit total pressure obtained from a manifold of eight total pressure tubes located inside the ejector was measured with a 15-psid transducer. The tunnel dynamic pressure and the model base pressure were measured with 1.0- and 0.3-psid transducers, respectively. The tunnel and ejector-exit total temperatures were measured with iron-constantan thermocouples.

SECTION III
PROCEDURE

3.1 DATA PROCUREMENT

In general, data were obtained at jet-to-free-stream velocity ratios of 0, 2.0, 3.3, and 4.5 for each tunnel wall configuration with the horizontal tail off and on. The nominal tunnel and model conditions corresponding to the velocity ratios are as follows:

V_R	q_∞	V_∞	V_j	Re x 10^{-5}
0.0	29.2	160	0	5.10
2.0	24.4	145	290	4.59
3.3	16.8	120	396	3.79
4.5	16.8	120	540	3.79

Test conditions were selected to match as close as practicable those of the interference-free data. However, in order to avoid the necessity of calibrating the test section for each wall configuration, it was assumed

that the tunnel calibration obtained with solid walls was not significantly affected by wall porosity.

The tunnel velocity was set by varying the fan speed until the desired dynamic pressure was established at the test section entrance. Since the tunnel temperature was not controllable, a "warm-up run" was made at the beginning of each test period to stabilize temperature. The tunnel dynamic pressure was adjusted to compensate for temperature changes if the temperature changed 10°F during the course of a test period which was about six hours duration. High-pressure nitrogen was supplied to the ejector through an appropriate pressure control system until the desired jet exit total pressure was obtained. The jet exit temperature was also uncontrollable. However, no adjustment was made for its variation. This procedure is justified by the fact that the aerodynamic forces, which were of primary interest, were not significantly affected by small changes in velocity ratio.

3.2 DATA PROCESSING

The instrument readings were transferred from hand recorded data sheets to paper tape and processed with a digital computer using standard data subroutines for computing the tunnel conditions, force and moment coefficients, and model parameters.

3.2.1 Determination of the Incident Correction Factors

For reasons to be discussed in Section IV, it is assumed that the correct angle of attack for a V/STOL model in a wind tunnel is given by

$$\alpha = \alpha_m + \delta \frac{S}{C} C_L + \Delta\alpha_j$$

where δ and $\Delta\alpha_j$ are constants for a given wall configuration and velocity ratio. Values of δ and $\Delta\alpha_j$ were obtained by comparison of data from the V/STOL tunnel with the assumed interference-free results from the LTV tunnel in the least-squares sense from the relations

$$\delta = \frac{C}{S} \frac{N \sum_1^N [f(C_{L_i}) - \alpha_i] C_{L_i} - \sum_1^N [f(C_{L_i}) - \alpha_i] \sum_1^N C_{L_i}}{N \sum_1^N C_{L_i}^2 - (\sum_1^N C_{L_i})^2} \quad (1)$$

and

$$\Delta\alpha_j = \frac{\sum_1^N [f(C_{L_i}) - \alpha_i] \sum_1^N C_{L_i}^2 - \sum_1^N [f(C_{L_i}) - \alpha_i] C_{L_i} \sum_1^N C_{L_i}}{N \sum_1^N C_{L_i}^2 - (\sum_1^N C_{L_i})^2} \quad (2)$$

Equations (1) and (2) are derived in Appendix II.

The incident correction is a coordinate rotation of the force components in the pitch plane from an axis determined by the tunnel centerline to an axis determined by the airstream direction related to the free air condition. The amount of the axis rotation ($\Delta\alpha$) is the difference between the geometric angle of attack in the wind tunnel and the equivalent free-air angle of attack. Thus,

$$\Delta\alpha = \alpha - \alpha_m$$

The corrected force coefficients are given by

$$C_L)_c = C_L \cos \Delta\alpha - C_D \sin \Delta\alpha \quad (3)$$

$$C_D)_c = C_L \sin \Delta\alpha + C_D \cos \Delta\alpha \quad (4)$$

In many instances, $\Delta\alpha$ and C_D are sufficiently small so that the correction to the lift coefficient is within the uncertainty interval of the data and may be neglected. Such was the case for the investigation reported herein.

3.3 DATA PRECISION

The data contained herein were determined from single-sample measurements. The uncertainties for the data are estimated from instrument precision and calibration curve-fit deviations. All uncertainties are based on a 95-percent confidence level. The precision of the measurements is as follows:

V_R	C_{L_f}	C_{D_f}	C_m	q_∞	V_R	α_m
0.0	±0.011	±0.006	±0.005	±0.3	---	±0.1
2.0	±0.009	±0.008	±0.005	±0.3	±0.01	±0.1
3.3	±0.017	±0.010	±0.008	±0.3	±0.03	±0.1
4.5	±0.022	±0.016	±0.008	±0.3	±0.04	±0.1

The accuracy of q_∞ is affected by the assumption that the tunnel calibration was unaffected by changes in wall porosity. Subsequent tunnel calibration with open horizontal walls (Ref. 15) has shown that the assumption was not appropriate. Thus, the accuracy of q_∞ is a function of wall porosity. If it is assumed that the variation of q_∞ for a given tunnel nozzle exit condition is a linear function of wall porosity, the accuracy of q_∞ with τ = 20 percent is within 0.3 to -0.54 psf.

The accuracy of V_R is affected by variations in the jet and the tunnel temperatures (neither of which was controllable) from one test period to the next. The test conditions were considered acceptable if the velocity ratio was within 0.1 of the desired value.

SECTION IV
RESULTS AND DISCUSSION

4.1 THEORETICAL CALCULATION OF THE INTERFERENCE VELOCITIES

Extensive theoretical calculations for wall corrections have been made for solid, slotted, perforated, and open test sections of various cross-sectional shapes. The solutions have been obtained by assuming a compressible or incompressible fluid which is inviscid and irrotational. The incompressible flow field in terms of the perturbation velocity potential is described by

$$\frac{\partial^2 \phi}{\partial x^2} + \frac{\partial^2 \phi}{\partial y^2} + \frac{\partial^2 \phi}{\partial z^2} = 0 \tag{5}$$

The velocity potential ϕ is considered to be the sum of the potential due to the model in free air ϕ_m and the interference potential caused by the presence of the tunnel boundary ϕ_i. The free-air model potential is represented by appropriate singularities dependent on the problem under consideration. For example, if it is assumed that the model is small compared to the tunnel size, a horseshoe vortex may be used to represent a lifting wing, and a doublet may be used to represent the blockage of a model. A combination of singularities has been used to represent more complicated configurations. The solution for ϕ_i is obtained by satisfying the boundary condition which is determined by the wind tunnel under consideration. For a solid wall, the velocity normal to the wall must be zero. The perturbation potential is zero at the boundary of an open tunnel. For a slotted tunnel, which is of interest in this report, the boundary condition

$$\phi + K \frac{\partial \phi}{\partial n} = 0 \tag{6}$$

has been derived by several authors (Refs. 17 through 21) by replacing the slotted boundary with an equivalent homogeneous boundary. The parameter K is related to the slot spacing and wall porosity and is discussed in more detail in Section 4.4.2.

It has been found convenient to correlate the theoretical results by a slot parameter P defined as

$$P = \left[1 + \frac{K}{h}\right]^{-1} \tag{7}$$

A closed wall corresponds to P = 0, whereas an open wall is represented by P = 1.

4.2 INTERFERENCE-FREE DATA

The lift data obtained in the LTV tunnel are presented in Fig. 6. It should be noted that the forces being considered do not contain the direct force from the ejector and its inlet, but only the forces caused by flow over the model. The lift coefficient fairings were obtained from a least-squares curve fit of each set of data. The data exhibit a decrease in the aerodynamic lift at a given angle of attack as the velocity ratio is increased. The lift decrement, which is characteristic of V/STOL configurations, is caused by the flow field induced by the jet and its inlet. The induced flow field is essentially normal to the model planform, thereby causing a negative normal force. The lift data for each velocity ratio show a slight Reynolds number dependence.

The drag data (shown in Fig. 7) indicate an increase in drag, at a constant value of the lift coefficient, as the velocity ratio increases. The increased drag may be attributed to two factors. First, as the jet velocity is increased, at a constant free-stream condition, the velocity of the jet-induced flow field over the model increases causing an increase in the drag force. However, the drag data are nondimensionalized with the free-stream dynamic pressure. Thus, the drag coefficient is computed from an increased value of the drag without compensating for the jet-induced increase in the dynamic pressure. Secondly, the jet efflux has a highly turbulent characteristic. As its velocity increases, the influence of the turbulent flow on the model boundary layer is such to cause transition from laminar to turbulent conditions over a greater portion of the model, thereby increasing the skin friction. The drag data also exhibit an increased Reynolds number dependence as the velocity ratio is increased, which may be attributed to an increase in the susceptibility of the boundary to transition under the influence of the jet-induced free-stream turbulence as Reynolds number increases. It would have been interesting to obtain interference-free data with the location of the model boundary layer transition fixed.

The jet-induced flow field causes a severe nose up pitching moment, as shown in Fig. 8, which is inadequately compensated for by the force on the tail surface. The data are very Reynolds number dependent. In general, the pitching moment increases with decreasing Reynolds number, but at V_R of 4.5, the data display a rather erratic behavior. A very brief tuft investigation of the flow over the model indicated the presence of a vortex on the underside of the fuselage immediately behind the jet. It is probable that the vortex would be somewhat unstable with its position influenced by small changes in the flow field. Thus, the pitching moment data would show a greater influence of small flow field changes, reflected in Reynolds number, than would drag or lift.

4.3 BLOCKAGE INTERFERENCE

The V/STOL configurations are characterized by the presence of a skewed wake rather than a horizontal wake as in the case of conventional aircraft. The presence of a skewed wake in conjunction with the wind tunnel wall effects results in interference velocities in both the vertical and horizontal directions. The velocity encountered by a model in the wind tunnel is

$$U = [(U_\infty + u)^2 + v^2 + w^2]^{1/2} \tag{8}$$

where u, v, and w are the interference velocity components at the model caused by the presence of the tunnel boundaries. For most model configurations, v is identically zero because of flow field symmetry. Equation (8) may be written as

$$U = U_\infty \left[\left(1 + \frac{u}{U_\infty} \right)^2 + \left(\frac{w}{U_\infty} \right)^2 \right]^{1/2} \tag{9}$$

Theoretical formulations (Ref. 22) have led to the definitions of the upwash and streamwise interference factors for the case of a helicopter, lifting jet, or lifting fan as

$$\delta_w = \frac{w}{w_o} \frac{C}{A} \tag{10}$$

and

$$\delta_u = \frac{u}{w_o} \frac{C}{A} \tag{11}$$

respectively. The lift produced by the direct lift device can, from momentum considerations, be expressed as

$$L = 2\rho w_o U_\infty A \tag{12}$$

The lift from a wing is given by

$$L = 1/2\,\rho\, U_\infty^2 C_L S \tag{13}$$

Equating Eqs. (12) and (13) gives an expression for the reference velocity w_o in terms of an equivalent wing,

$$w_o = 1/4\, U_\infty C_L \frac{S}{A} \tag{14}$$

Substituting Eq. (14) into Eqs. (10) and (11) and in turn substituting into Eq. (9) yields an expression for the velocity at the model in terms of the interference factors

$$U = U_\infty \left[\left(1 + 1/4\,\delta_u \frac{S}{C} C_L\right)^2 - \left(1/4\,\delta_w \frac{S}{C} C_L\right)^2\right]^{1/2} \tag{15}$$

An experimental method for independently evaluating δ_U and δ_W for a V/STOL configuration has not been devised. An estimate of U/U_∞, however, may be obtained from theoretical solutions. It is shown in Ref. 8 that δ_U and δ_W have maximum values of 0.3 and 0.8, respectively, for the V/STOL tunnel configuration. For the investigation reported herein, $C_L \leq 1$ and $S/C = 0.133$. Thus, U/U_∞ has a maximum value of 1.01 which occurs with a solid test section. As the porosity of the tunnel is increased, the value of U/U_∞ decreases to a minimum value of 0.99 with the horizontal walls open. Further, theory indicates that at the condition of zero upwash interference, the blockage correction is also near zero. Thus, the primary objective of the investigation, that of searching for a minimal interference configuration, is not compromised by neglecting the blockage correction. Therefore, the velocity approaching the model was taken from the tunnel calibration results.

4.4 UPWASH INTERFERENCE

4.4.1 Theoretical Considerations

The change in angle of attack of a lifting body caused by the presence of the tunnel walls may be expressed, in terms of the perturbation velocities, as

$$\Delta\alpha = \tan^{-1} \frac{w}{U_\infty + u} \approx \frac{w/U_\infty}{1 + u/U_\infty} \tag{16}$$

Substituting Eq. (14) into Eqs. (10) and (11) and in turn substituting into Eq. (16) gives the change in angle of attack of a V/STOL vehicle due to the presence of the wind tunnel walls as

$$\Delta\alpha = \frac{1/4\ \delta_w \frac{S}{C} C_L}{1 + 1/4\ \delta_u \frac{S}{C} C_L} \tag{17}$$

By using the values given in the previous section, the term $1/4\ \delta_u\ C_L\ S/C$ has a maximum value of 0.01 which may be neglected compared to one. Thus, Eq. (17) can be written in the form of the classical correction equation

$$\Delta\alpha = \delta \frac{S}{C} C_L \tag{18}$$

The factor δ is commonly referred to as the lift interference factor.

Experimental results (Ref. 7) have indicated that an additional correction is needed in the V/STOL case - at least for a model for which part of the lift is due to aerodynamic surfaces. Not only do the tunnel walls introduce an interference potential into the flow field, but they also cause a change in the trajectory of the jet wake. As a result, the jet-induced flow field over the model is different than in the free-air case. It was observed that the effect could be compensated for by an additional incident correction term which is independent of lift. The incident correction then becomes

$$\Delta\alpha = \delta \frac{S}{C} C_L + \Delta\alpha_j \tag{19}$$

where $\Delta\alpha_j$, termed the jet interference angle, is an angle-of-attack increment to account for the change in the jet-induced flow field over the model. It is shown in subsequent portions of this report that $\Delta\alpha_j$ is a function of jet-to-free-stream velocity ratio and tunnel wall configuration. It is probable that $\Delta\alpha_j$ is also dependent on a model-to-tunnel size parameter and model configuration. It appears that a theoretical evaluation of the term would require detailed knowledge of the induced flow field of a jet in crossflow, a capability which is currently beyond the state of the art. Nevertheless, all experimentally determined interference quantities have been computed from Eq. (19) in the least-squares sense as described in Section III using the aerodynamic rather than the total lift coefficient. The procedure is valid because the tests were conducted at constant values of jet thrust and justified because the aerodynamic lift measurement is significantly more accurate than the total lift (due to piping interactions). Thus, the addition of a constant increment to both the interference and interference-free data does not

change the relationship between the two sets of data. Therefore, the interference factors are unaffected. The interference factors computed from the data obtained with the model tail off and on were essentially the same. Therefore, no distinction is made between the two model configurations in the discussion of incident corrections.

4.4.2 Comparison between Theory and Experiment

It is indicated in Ref. 7 that theory and experiment were in qualitative rather than quantitative agreement. Part of the discrepancy in the data of Ref. 7 was caused by not taking into account the change in tunnel calibration as the horizontal wall porosity was increased. It is shown in Ref. 15 that the test section velocity with horizontal walls open is significantly different from the solid-wall calibration. The data have been corrected by assuming that the variation in the calibration is linear with wall porosity so that, for example,

$$C_L)_C = \frac{q_{solid}}{q_\tau} \quad C_L \tag{20}$$

where $q_\tau = q_{solid} + \tau(q_{open} - q_{solid})$. The corrected data are shown in Fig. 9. Theory and experiment are in good agreement for the closed and open tunnel but do not agree for the slotted case. The reason for the disagreement lies in the expression for K in Eq. (6), which relates the wall geometry to the boundary condition. The expression for K used in Ref. 7,

$$K_1 = \frac{\ell}{\pi} \ell_n \csc \frac{\pi}{2} \frac{a}{\ell} \tag{21}$$

has been derived independently in Refs. 17, 18, 19, and 20 and has been used in most publications concerning slotted-wall interference. A second expression for the boundary parameter

$$K_2 = -\frac{\ell}{2}\left(1 - \frac{a}{\ell}\right) \frac{\cos \pi\left(1 - \frac{a}{\ell}\right) - \cosh \frac{\pi t}{\ell}}{\sin \pi\left(1 - \frac{a}{\ell}\right)} \tag{22}$$

derived in Ref. 21 results in a much better correlation between theory and experiment as shown in Fig. 10.

Equation (21) was derived using conformal transformation techniques and by replacing the slotted wall with an imaginary homogeneous boundary. Flow through the equivalent boundary may be described by the potential expression for flow through a thin screen with parallel

equidistant slits. Equation (22) was derived by representing the slats in the tunnel wall by rod doublets. The strength of the doublet is evaluated in terms of the slat width, thickness, and spacing by considering the flow normal to the wall to have a stagnation point at the center of each slat. Apparently, the rod-doublet representation of the slotted wall is closer to the physical flow field than the mathematical model used to derive Eq. (21).

It is surprising that the theoretical and experimental data obtained at $V_R = 4.5$ agree so well since the jet intersects the tunnel floor in such close proximity to the model (see Fig. 1). However, since theory and experiment agree well for the closed and open horizontal walls, P_{2_H}, of zero and one, respectively, it would appear that the lack of agreement is associated with the boundary expression rather than the theoretical model or the nearness of the jet impingement point.

The effect of slots in the vertical walls on the lift interference is shown in Fig. 11. The experimental data have been corrected by Eq. (20) for the change in tunnel calibration caused by ventilating the test section. The theory and experiment agree quite well. As would be expected, vertical wall porosity is not as effective in reducing upwash interference as is porosity in the horizontal walls. The penalty paid for using a porous wall is increased power loss, test section noise, and turbulence. Thus, it is desirable to keep the test section porosity as small as possible. Consequently, all subsequent wall configurations tested had solid vertical walls.

All theoretical formulations to data assume a constant slot width extending to infinity upstream and downstream. As will be shown in the following paragraphs, in order to minimize other types of interference, it is desirable to consider a slot configuration which varies the slot width with position. For these cases, a direct correlation between theory and experiment is not applicable. Further, the jet interference angle ($\Delta\alpha_j$) is not considered in the theoretical treatment. It was found that the interference factors δ and $\Delta\alpha_j$ for a given slot shape may be represented by a single curve when presented versus test section porosity. A typical example using the data obtained with Configuration A is shown in Figs. 12 and 13. All subsequent data comparisons will be made with porosity as the correlating parameter.

4.4.3 Effect of Configuration on the Incident Correction Factors

The variation of the lift interference factor with porosity is presented in Fig. 14 for each slot configuration. The data points have been

omitted for clarity. The data for Configurations A, B, and C may be represented by a single curve. Since the Configuration A data agreed with theory, the data obtained with Configurations B and C will also agree with theory provided the average value of the slot width is used in Eq. (19).

Since the effect of an element of slot is proportional to the inverse of its distance from the model, it would be expected that the open area near the entrance of the test section would have a smaller influence on the interference at the model than the porosity near the model. The expectation is realized by the fact that at every velocity ratio the porosity required for a given value of the interference parameter is less than with Configurations D through G than with Configurations A, B, or C.

For velocity ratios greater than zero, the variation of porosity with Configurations E and F was accomplished by changing the width of the slot just above and below the model. The porosity for zero interference was further reduced compared to previous configurations for each velocity ratio. It is surprising that Configurations E and F resulted in an identical variation of δ with porosity. It will be recalled from Section II that the increase in porosity with the Configuration F was obtained by opening the area just under the jet, whereas Configuration E opened the region above and below the jet for the rear half of the test section. Thus, the data would seem to indicate that the open area behind the model does not have a large influence on the lift interference factor as might be expected because of the distance involved. However, the Configuration G, which increased porosity by opening only the rear third of the test section, produced a variation of δ opposite other configurations. The reason for the anomaly is unknown.

Theoretical results (Ref. 9) show that certain combinations of top and bottom wall porosity will not only result in zero upwash interference but will also remove the velocity ratio dependence. Configuration G is of the wall type suggested in Ref. 9. While the variation of δ with τ is opposite the other configurations, the data for all three velocity ratios tested are almost coincidental. Thus, additional work with configurations with small porosity on the top wall and moderate values of porosity on the bottom wall is warranted.

The variation of the jet interference angle ($\Delta\alpha_j$) with porosity for the various wall configurations is presented in Fig. 15. The value of $\Delta\alpha_j$ for the classical case, $V_R = 0$, is identically zero. Except where porosity variations were insufficient, each wall configuration resulted in a variation of $\Delta\alpha_j$ with τ which passed through zero. As with δ, the

porosity required for zero $\Delta\alpha_j$ with a given wall configuration increased with increasing velocity ratio. Also, Configurations E and F required the smallest value of porosity to eliminate the interference.

Unfortunately, at almost all conditions, the porosity required for zero δ is different from that required for zero $\Delta\alpha_j$ as shown in Fig. 16. It will be recalled from Fig. 4 that Configurations A through D had a slat directly above and below the jet. Data obtained with the centerline slat removed showed no effect on the variation of δ with porosity, but caused $\Delta\alpha_j$ to be negative. The data with Configuration A, shown in Fig. 17, are a typical example. Although there is a strong interaction, the results suggest that δ is primarily a function of porosity while $\Delta\alpha_j$ is primarily a function of the transverse distribution of porosity. Configurations E and F, which only varied the width of the center slot, were an attempt to use this result to simultaneously reduce δ and $\Delta\alpha_j$ to zero. Comparison of the Configuration E and F curves (Fig. 16) shows that, except in the neighborhood of $V_R = 3$, the centerline slot is much too open. Thus, it is suggested that the proper configuration to simultaneously give zero δ and $\Delta\alpha_j$ would have a transverse porosity gradient proportional to the local value of the downwash. The total porosity should not be significantly different from that required for zero δ with Configuration E or F.

4.4.4 Effect of Configuration on Drag

The drag data obtained with a closed test section and with open horizontal walls at velocity ratios of zero and 4.5 are presented in Fig. 18a. The drag coefficients obtained with other wall configurations lie between the data obtained with these two extreme configurations. The corrected data (Fig. 18b) were calculated from Eqs. (4) and (19) using the values of δ and $\Delta\alpha_j$ determined from Eqs. (1) and (2).

The corrected data for the closed test section agree very well with the interference-free data. However, the data obtained with open horizontal walls are increased by a constant drag increment, resulting in the corrected data being parallel to the interference-free curve. The data offset may be attributed to a change in the test section flow quality resulting from an increase in free-stream turbulence with the open walls. The increased free-stream turbulence causes the model boundary layer to transition earlier, thus increasing skin friction, hence drag. It is interesting to note that the drag increment is less at $V_R = 4.5$ than at $V_R = 0$. This phenomenon may be attributed to the fact that the jet efflux which, in itself, is highly turbulent, dominates the flow field particularly on the underside of the model. Thus, the jet causes a substantial part of the model boundary layer to become turbulent lessening the effect of free-stream turbulence.

The data shown in Fig. 18 indicate that the drag data may be corrected by a simple rotation of the wind axis caused by the lift-induced change in incidence. Thus, a wall configuration which has zero incident correction will produce interference-free drag data, provided flow quality is not a factor.

4.5 AXIAL GRADIENT OF INTERFERENCE

4.5.1 Theoretical Consideration

Classically, pitching moment data have been corrected because of "streamline curvature" which results because the wall-induced velocities are not constant in the axial direction. For an airfoil, the interference effect can be considered to be a change in chamber. Corrections to the pitching moment are derived from lifting line theory, assuming a circular airfoil and that the interference factor δ is linear in the axial direction (Ref. 23). The assumptions are reasonable provided the chord is small compared to the tunnel dimensions. The correction to pitching moment for an airfoil in a rectangular tunnel (Ref. 24) is

$$\Delta C_m = \frac{\tau S}{32\, hC} C_L \frac{\partial \delta}{\partial x} \frac{\partial C_L}{\partial \alpha} \tag{23}$$

In the case of a model with a horizontal tail, the tail experiences a different angle of attack, because of wall interference, in a wind tunnel than in free air. The dynamic pressure at the tail will also be different in the wind tunnel than in free air. The correction to the pitching moment derived for a V/STOL model with a horizontal tail (Ref. 25) is

$$\Delta C_m = \frac{q_T}{q_w} \frac{S_T}{S_w} \frac{x'}{\bar{c}_w} \frac{\partial C_{L_T}}{\partial \alpha_T} (\Delta \alpha_w \Big| - \Delta \alpha_T) \tag{24}$$

where $\Delta\alpha$ is defined by Eq. (19) with the proper subscripts depending on whether the wing or tail is being considered. The evaluation of $\Delta\alpha_T$ requires independent measurement of the tail forces which was not done in the present investigation.

An additional factor should be considered in the evaluation of the pitching moment data. Partly because of the slotted walls and partly because of inherent tunnel qualities, the turbulence level in the V/STOL tunnel is relatively high. The high turbulence level would tend to speed boundary layer transition and delay separation of the flow over the model. Small changes in either quantity affect the pitching moment and drag more noticeably than lift. Thus, one would expect more anomalies

in the drag and pitching moment data than in the lift data. Unfortunately, the effect of free-stream turbulence cannot be readily evaluated and thus represents an unknown quantity in the data. Because of a nonuniform variation of the pitching moment data with wall configuration, the data are not suitable for mathematical treatment as were the lift and drag data. Therefore, one must regress to direct data comparisons.

The variation of pitching moment with lift for a closed test section, open horizontal walls, and Configuration A with δ approximately zero is shown in Fig. 19. It is evident that, for $V_R = 0$, Eq. (23) with an appropriate value of the interference factor can be used to correct the data. At $V_R = 4.5$, however, while a small correction proportional to lift may be inferred, the primary correction needed is a constant moment increment independent of lift. The data with $V_R = 4.5$ are typical of all the data for the V/STOL case, although, in general, the moment increment required to correct the data is a function of velocity ratio. Examination of Eq. (24) shows for a linear lift curve that to obtain a constant moment correction ($\Delta\alpha_w - \Delta\alpha_T$) must be constant. Since each term contains the incident correction factors δ and $\Delta\alpha_j$ at the appropriate location, it is not obvious that Eq. (24) will provide the desired result. Subsequent investigations should use a metric tail to resolve this question.

Theoretical solutions for the axial interference gradient (Ref. 7 for the classical case and Ref. 8 for the V/STOL case) show that with a closed wall the positive pitching moment should be less than free air, approach free air as the wall porosity increases, and finally, be greater than free air when the horizontal walls are fully open. Although, for the classical case (Fig. 19a), the experimental data first decrease and then increase with increasing porosity, the data generally agree with the predicted trends. In the V/STOL case (Fig. 19b) the pitching moment obtained with solid walls is less than the interference-free results as predicted, but C_m decreases with increasing porosity, opposing the theoretical prediction. Apparently, these results are caused by the flow field induced by the wake-wall interaction which has been shown to result in complicated vortex-like flow patterns (Refs. 12 and 26).

4.5.2 Effect of Wall Configuration on Pitching Moment

Wall Configurations B through G were tested in an attempt to influence pitching moment. In general, as indicated in Fig. 19, the wall configuration which produced near zero upwash interference produced large pitching moment deviations. In the classical case, $V_R = 0$, fairly

good agreement with interference-free data was obtained with Configurations D and E with the lift interference factor approximately zero as shown in Fig. 20. However, the pitching moment data show a substantially different variation with lift in the V/STOL tunnel than was found in the LTV tunnel. It was shown previously that the pitching moment is Reynolds number sensitive. It is felt that the basic difference in curve shape shown in Fig. 20, which is typical of all the data, may be attributed to different transition-point location in the V/STOL tunnel. The change in transition location is caused by a higher free-stream turbulence in the V/STOL tunnel which is equivalent to a Reynolds number effect. Insufficient data were taken to evaluate the effect of Reynolds number between the two tunnels.

The difference between tail-on and tail-off pitching moment for the data of Fig. 20 is shown in Fig. 21. The agreement of the data from Configurations D and E with interference-free results indicates that there is no axial interference gradient with the two configurations for $V_R = 0$. Thus, with equal flow quality, tests of conventional aircraft configurations in a slotted tunnel with slots matching Configuration D with $\tau = 3$ percent or Configuration E with 2.14-percent porosity should duplicate free air lift, drag, and pitching moment results.

The degree of difficulty in simultaneously eliminating lift and pitching moment interference is increased in the V/STOL case because $\Delta\alpha_j$ must also be forced to zero. As indicated in Fig. 16, data were seldom obtained with a configuration which produced zero incident correction; that is, $\delta = \Delta\alpha_j = 0$. Thus, in general, the wall configurations which produced interference-free pitching moment must be further modified to satisfy the upwash interference requirements.

It was indicated in Fig. 19 that the pitching moment data obtained in the V/STOL tunnel with various wall configurations tended to be too negative. However, two configurations were found which resulted in pitching moment data that were in fairly good agreement with the interference-free results at a velocity ratio of two. As shown in Fig. 22, the data with Configuration D with $\tau = 8$ percent and Configuration G with $\tau = 8.2$ percent agree well with the LTV data except at positive lift with the tail on. The effect on pitching moment of varying the width of the centerline slot, Configuration E, is shown in Fig. 23. It is seen that the greatest effect of the configuration on the data is at positive lift with the tail on. As the width of the centerline slot is increased, the data at positive lift with the tail on approach the interference-free results, whereas the remainder of the data is relatively unaffected. Thus, it would appear that increasing the center slot width of Configurations D and E would result in excellent agreement of the pitching moment data over the complete angle-of-attack range of the test.

Since the jet-wall intersection region at V_R = 3.3 and 4.5 is in close proximity to the tail (Fig. 1), the pitching moment is dominated by the wake-boundary interaction. The only configuration which drastically modified the wake impingement region, Configuration G, also resulted in the highest pitching moments for velocity ratios of 3.3 and 4.5. The data are presented in Fig. 24 along with that obtained with Configuration D with $\delta \approx 0$, which is typical of other configurations. It is evident that Configuration G resulted in a significant improvement in the pitching moment in each case - thus indicating that future investigations should consider further modifications in the wake impingement region.

SECTION V
CONCLUSIONS

An investigation of wind tunnel wall interference with a jet-in-fuselage model has resulted in the following conclusions:

1. Theory and experiment are in acceptable agreement for the classical case provided an appropriate expression is used to represent the tunnel boundary characteristics. While the theoretical and experiment lift interference factors agree well in the V/STOL case for a closed and open horizontal wall tunnel configuration, the boundary expression valid for classical models needs to be modified to obtain better quantitative agreement for slotted wall configurations with V/STOL models. The classical boundary expression does, however, give satisfactory qualitative results for the V/STOL case.
2. Classical data-correction equations are not appropriate for V/STOL configurations because of changes in the jet-induced flow field over the model. The effect of the tunnel boundary on the jet-induced flow field may be represented by an incident correction term ($\Delta\alpha j$), but its value must be determined empirically. Additional work, both theoretical and experimental, is needed to fully understand the implications of the jet interference angle in V/STOL model testing.
3. Although secondary interactions exist, the results of the investigation reported herein indicate that, for a given velocity ratio, the lift interference factor is primarily

a function of the test section porosity, the jet interference angle of the transverse distribution of porosity and pitching moment interference of the axial porosity gradient.

4. Two test section wall configurations (D with τ = 3 percent and E with τ = 2.1 percent) will, when the flow quality is equal, produce interference-free force and moment data for conventional aircraft configurations.
5. For the V/STOL case, Configuration D, modified so that the area directly under the jet is a little more open and by using a porosity which varies with velocity ratio, should result in interference-free data to a velocity ratio of two. Interference-free lift and drag data may be obtained at velocity ratios greater than two by simply increasing porosity. However, additional development is required to obtain interference-free pitching moment data at velocity ratios greater than two.
6. In general, the porosity required for zero interference is a function of velocity ratio. However, theory and a limited amount of experimental data indicate that a zero interference configuration with porosity independent of velocity ratio should be possible by using configurations which have a different porosity on the top and bottom walls. Therefore, future work should concentrate on configurations of that type. Additional attention should also be given to the area of the wake-wall intersection. Modification of the theory to consider axial gradients of porosity would also be helpful in the search for a minimal interference configuration for all model conditions.

REFERENCES

1. Anscombe, H. and Williams, J. "Some Comments in High-Lift Testing in Wind Tunnels with Particular Reference to Jet-Blowing Models." Advisory Group for Aeronautical Research and Development Report 63, North Atlantic Treaty Organization, Paris, August 1956.

2. Kuhn, Richard E. and Naeseth, Roger L. "Tunnel Wall Effects Associated with VTOL/STOL Model Testing." Presented to the Wind Tunnel and Model Testing Panel of AGARD, Brussels, Belgium, March 2-5, 1959.

3. Heyson, Harry H. "Jet Boundary Corrections for Lifting Rotors Centered in Rectangular Wind Tunnels." National Aeronautics and Space Administration TR-R-71, Washington, D. C., 1960.

4. Kirkpatrick, D. L. I. "Wind Tunnel Corrections for V/STOL Model Testing." Master's Thesis, University of Virginia, Charlottesville, Virginia, August 1962.

5. Olocott, John W. "A Survey of V/STOL Wind Tunnel Wall Corrections and Test Techniques." Princeton University Department of Aerospace and Mechanical Sciences Report No. 725, Princeton, New Jersey, 1965.

6. Lo, C. F. "Method of Calculating the Wind Tunnel Interference for Steady and Oscillating Wings in Tunnels of Arbitrary Wall Configuration." AEDC TR-68-42 (AD667187), March 1968.

7. Lo, C. F. and Binion, T. W., Jr. "A V/STOL Wind-Tunnel Wall Interference Study." Journal of Aircraft, Vol. 7, January-February 1970, pp. 51-57.

8. Lo, Ching-Fang. "Wind Tunnel Boundary Interference on a V/STOL Model." AIAA Paper No. 70-575, Presented at the Fifth Aerodynamic Testing Conference, Tullahoma, Tennessee, May 18-20, 1970.

9. Lo, Ching-Fang. "Test Section for a V/STOL Wind Tunnel." Journal of Aircraft, Vol. 7, July-August 1970, pp. 380-382.

10. Goethert, Bernhard H. Transonic Wind Tunnel Testing. Pergamon Press, New York, 1961.

11. Rae, W. H., Jr. "Limits on Minimum Speed V/STOL Wind Tunnel Tests." Journal of Aircraft, Vol. 7, August-September 1967, pp. 249-254.

12. Lazzeroni, F. A. and Carr, L. W. "Problems Associated with Wind Tunnel Tests of High-Disc-Loading Systems and Low Forward Speeds." Proceedings of the Third CAL/AVLABS Symposium, Aerodynamics of Rotary Wing and V/STOL Aircraft. Vol. II, Wind Tunnel Testing. The U. S. Army Aviation Material Laboratories and Cornell Aeronautical Laboratory, Inc., Buffalo, New York, June 18-20, 1969.

13. Margason, Richard M. "The Path of a Jet Directed at Large Angles to a Subsonic Free Stream." NASA TN-D-4919, November 1968.

14. Holbrook, J. W. "Low Speed Wind Tunnel Handbook." Ling-Temco-Vought Publication No. AER-EOR-12995-A, Dallas, Texas, March 1965.

15. Binion, T. W., Jr. "Description and Calibration of the AEDC Low Speed Wind Tunnel (V/STOL)." AEDC TR-70-266 (AD877999), December 1970.

16. Margason, Richard J. and Gentry, Carl L. "Static Calibration of an Ejector Unit for Simulation of Jet Engines in Small Wind-Tunnel Models." NASA TN-D-3867, March 1967.

17. Guderley, Gottfried. "Simplifications of the Boundary Conditions at a Wind-Tunnel Wall with Longitudinal Slots." WADC-TR-53-150, April 1953.

18. Davis, Don D., Jr. and Moore, Dewey. "Analytical Studies of Blockage- and Lift-Interference Corrections for Slotted Tunnels Obtained by the Substitution of an Equivalent Homogeneous Boundary for the Discrete Slots." NACA RM-L53E07b, June 1953.

19. Baldwin, Barrett S., Jr., Turner, John B., and Knechtel, Earl D. "Wall Interference in Wind Tunnels with Slotted and Porous Boundaries at Subsonic Speeds." NACA TN-3176, May 1954.

20. Maeder, Paul F. and Wood, Albert D. "Transonic Wind Tunnel Test Section." Journal of Applied Mathematics and Physics, Vol. 7, 1956, pp. 177-212.

21. Chen, C. F. and Mears, J. W. "Experimental and Theoretical Study of Mean Boundary Conditions at Perforated and Longitudinally Slotted Wind Tunnel Walls." AEDC-TR-57-20 (AD144320), December 1957.

22. Wright, Ray H. "Test Sections for Small Theoretical Wind-Tunnel-Boundary Interference on V/STOL Models." NASA TR-R-286, August 1968.

23. Pope, Allen. Wind-Tunnel Testing. Second Edition. John Wiley and Sons, Inc., New York, 1954.

24. Pindzola, M. and Lo, C. F. "Boundary Interference at Subsonic Speeds in Wind Tunnels with Ventilated Walls." AEDC TR-69-47 (AD687440), May 1969.

25. Heyson, Harry H. "Equations for the Application of Wind Tunnel Wall Corrections to Pitching Moment Caused by the Tail of an Aircraft Model." NASA TN-D-3738, November 1966.

26. Binion, T. W., Jr. "Investigation of the Recirculation Region of a Flow Field Caused by a Jet in Ground Effect with Crossflow." AEDC-TR-70-192 (AD711665), September 1970.

APPENDIXES

I. ILLUSTRATIONS

II. EXPERIMENTAL INCIDENT CORRECTION FACTORS

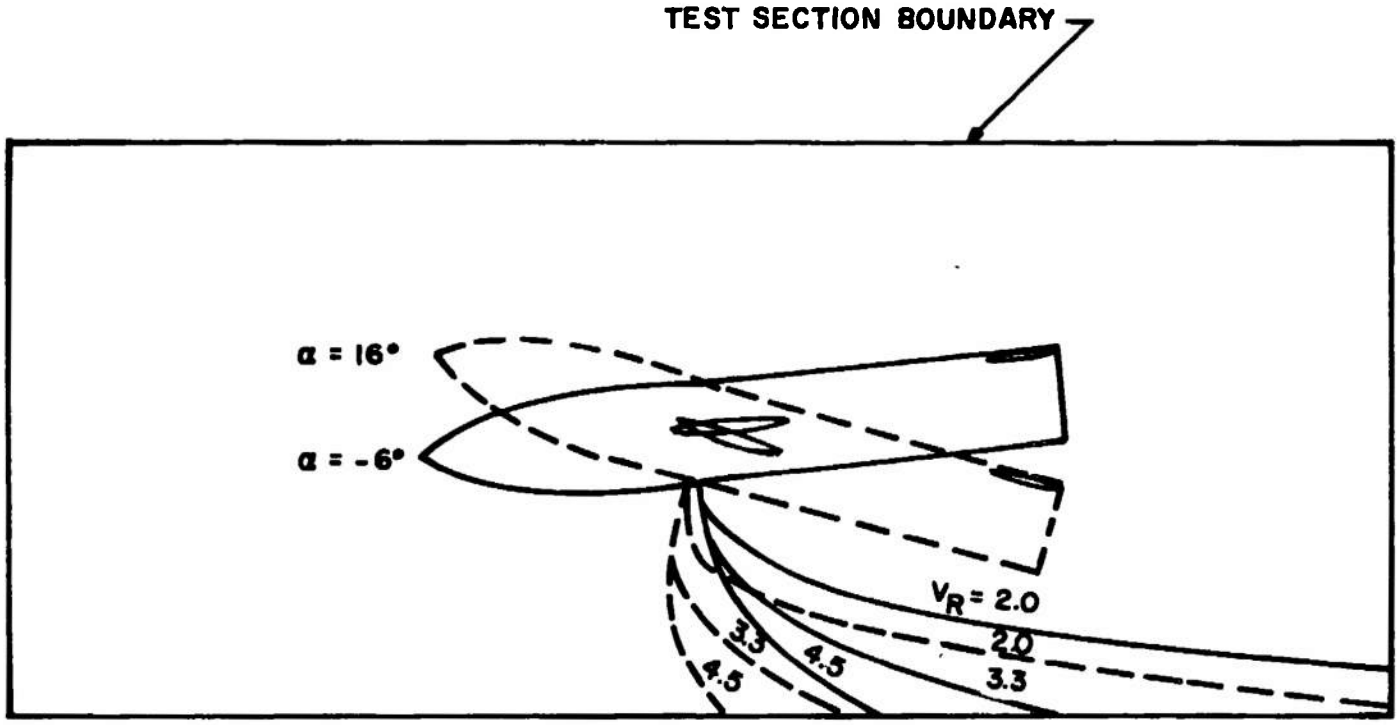

Fig. 1 Path of the Jet Wake

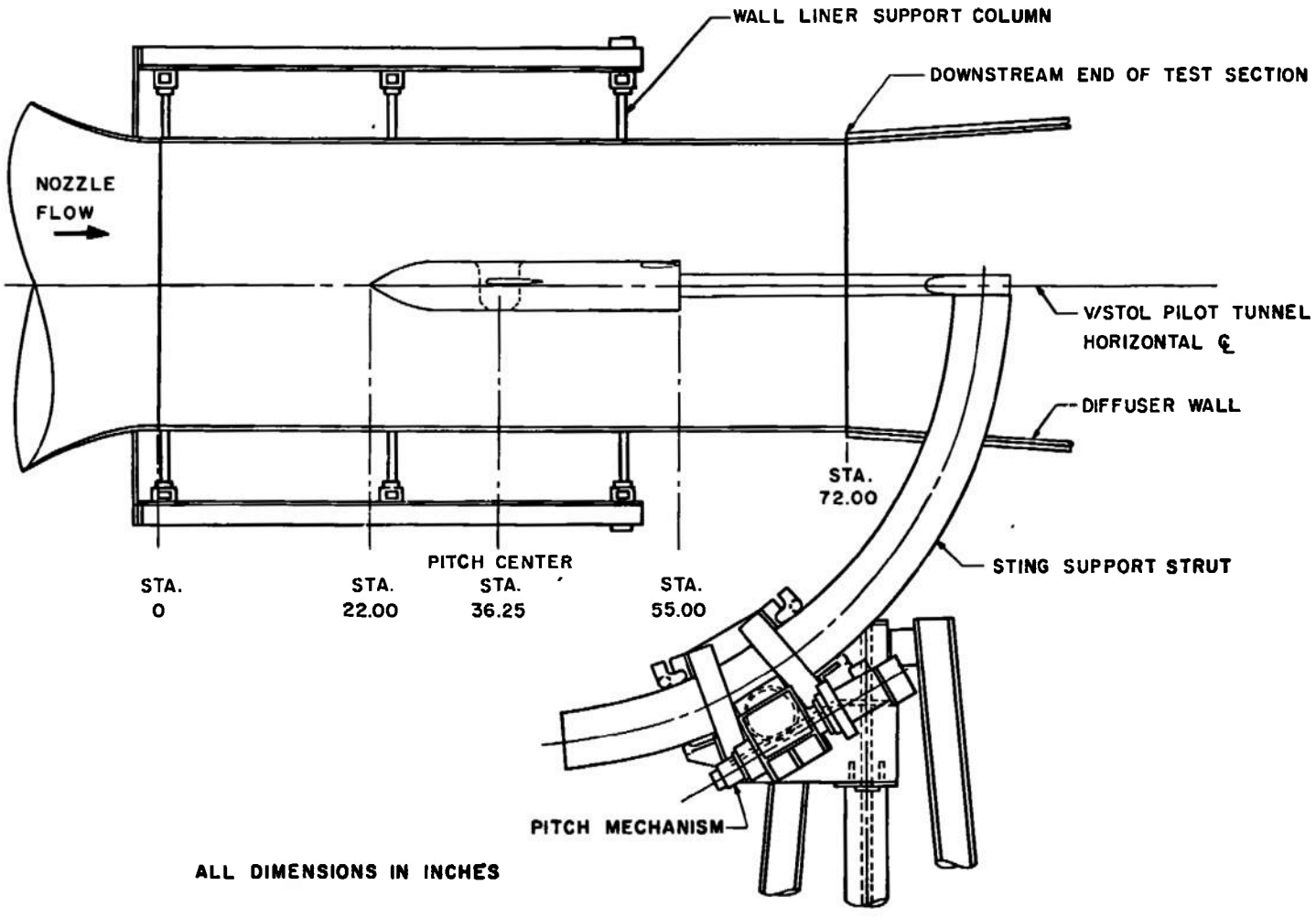

Fig. 2 Model Installation

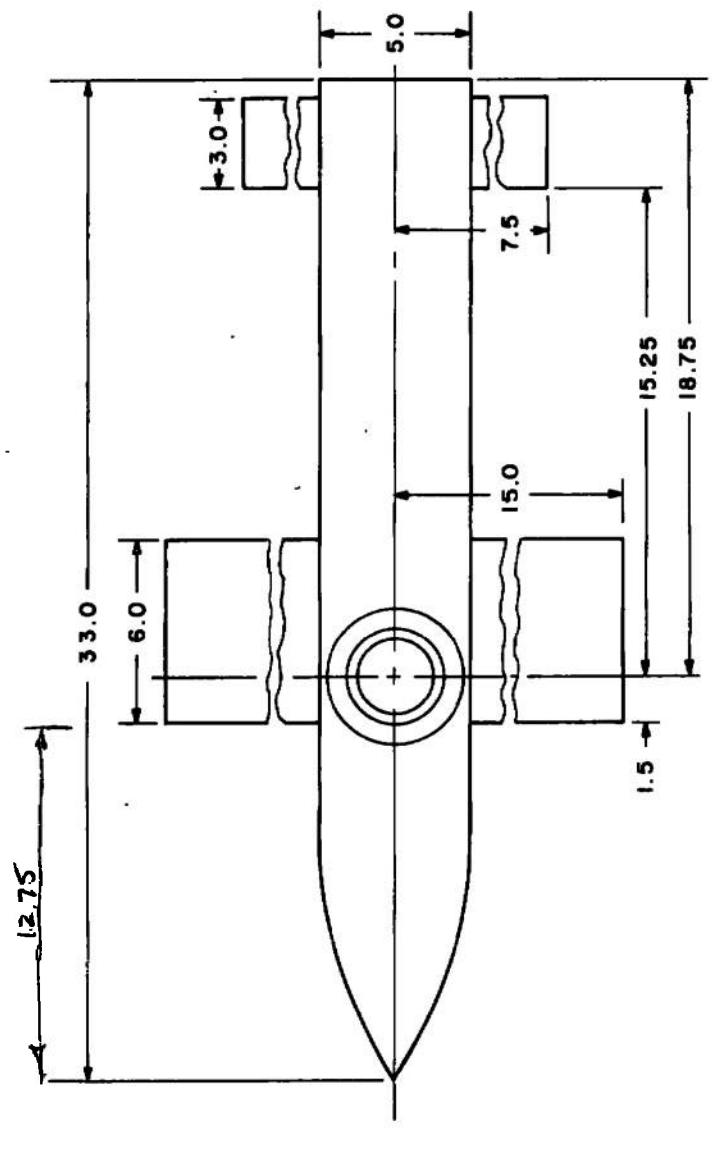

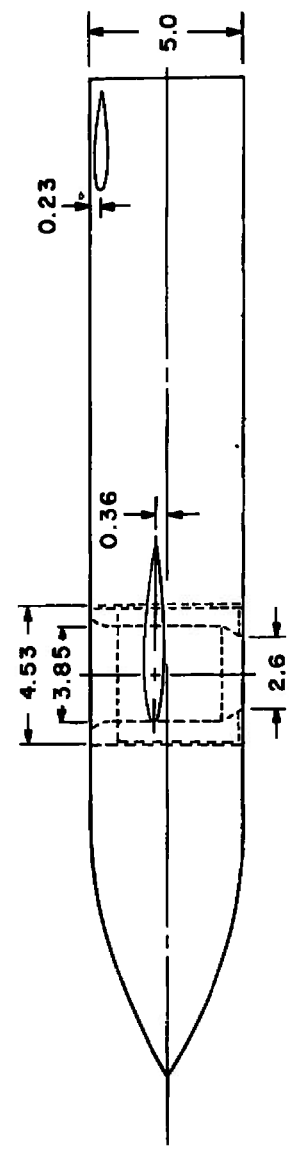

ALL DIMENSIONS IN INCHES

Fig. 3 Model Dimensions

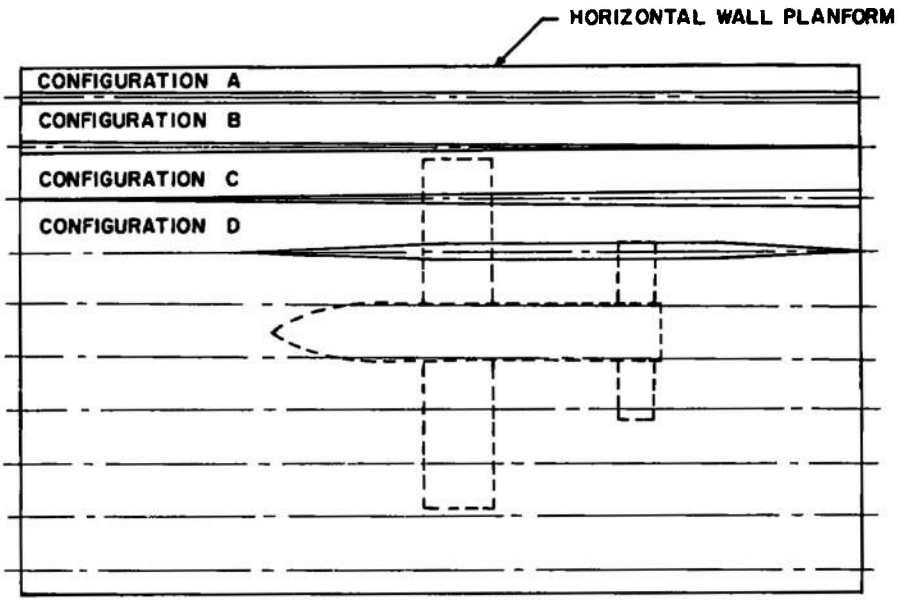

a. Slat on the Centerline

CENTERLINES INDICATE THE POSITION OF THE SLOT CENTERLINES FOR TEN SLOTS IN EACH HORIZONTAL WALL

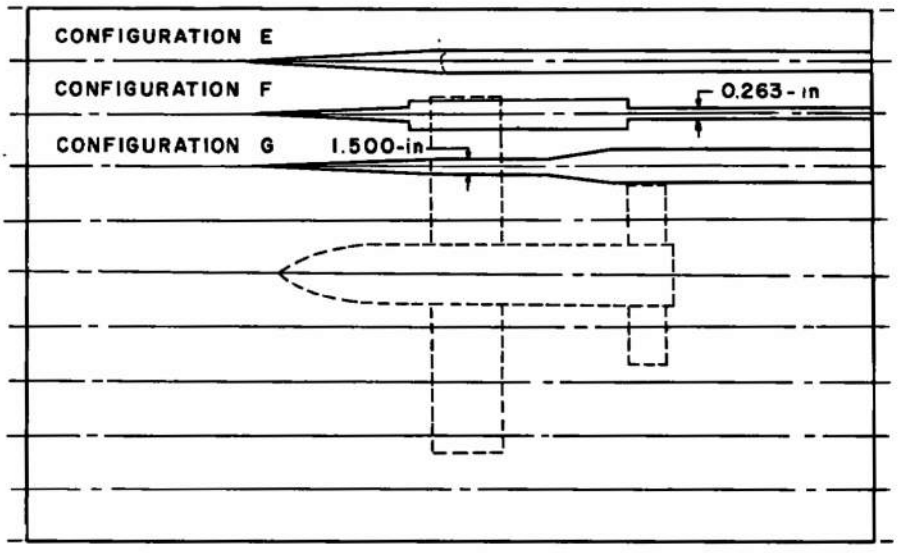

b. Slot on the Centerline

Fig. 4 Slot Geometry

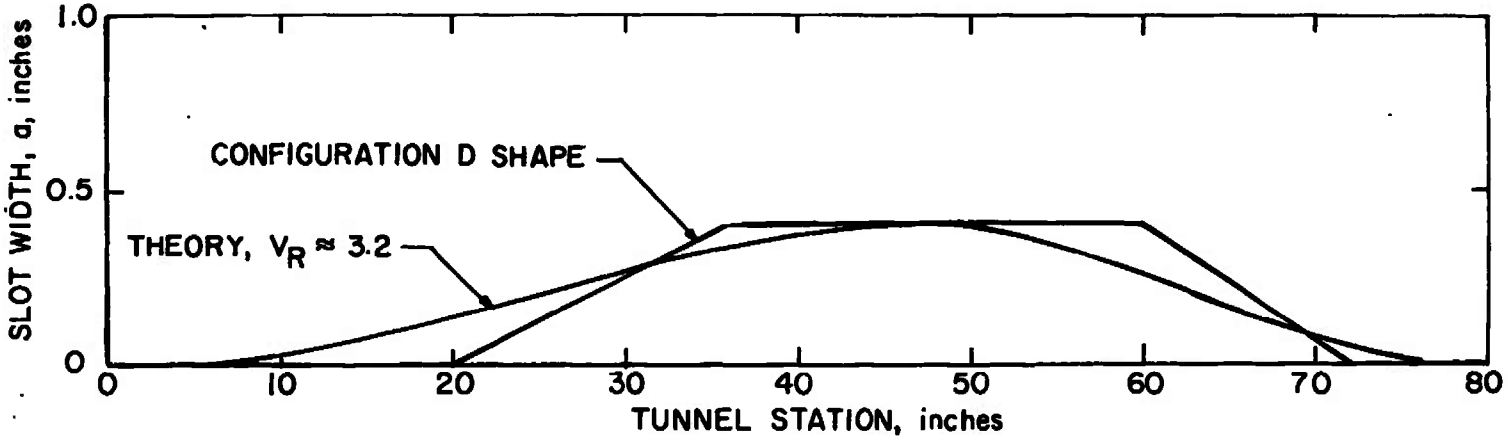

Fig. 5 Theoretical Slot Shape for Zero Axial Upwash Gradient

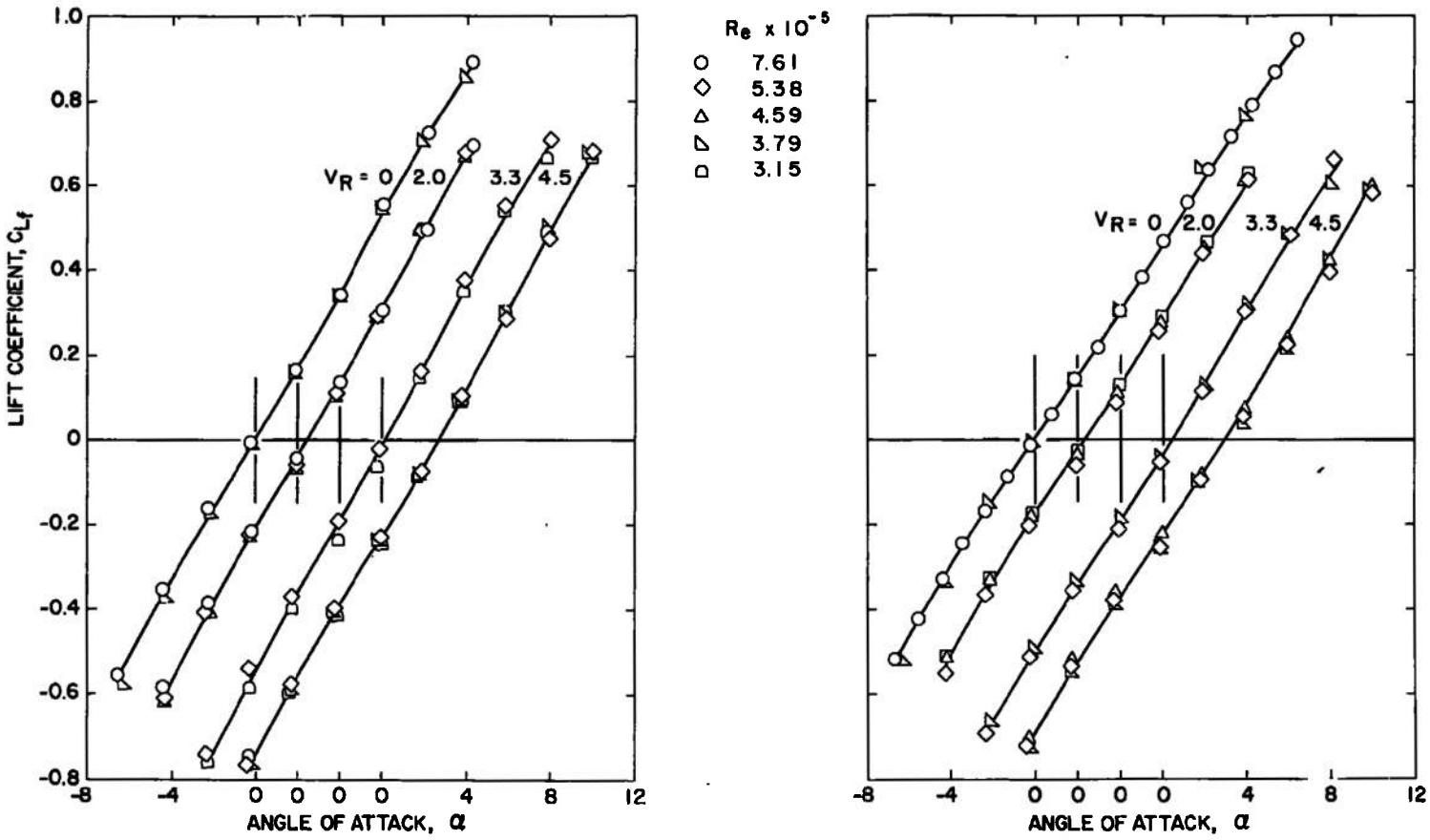

a. Tail-On

b. Tail-Off

Fig. 6 Interference-Free Lift Coefficient

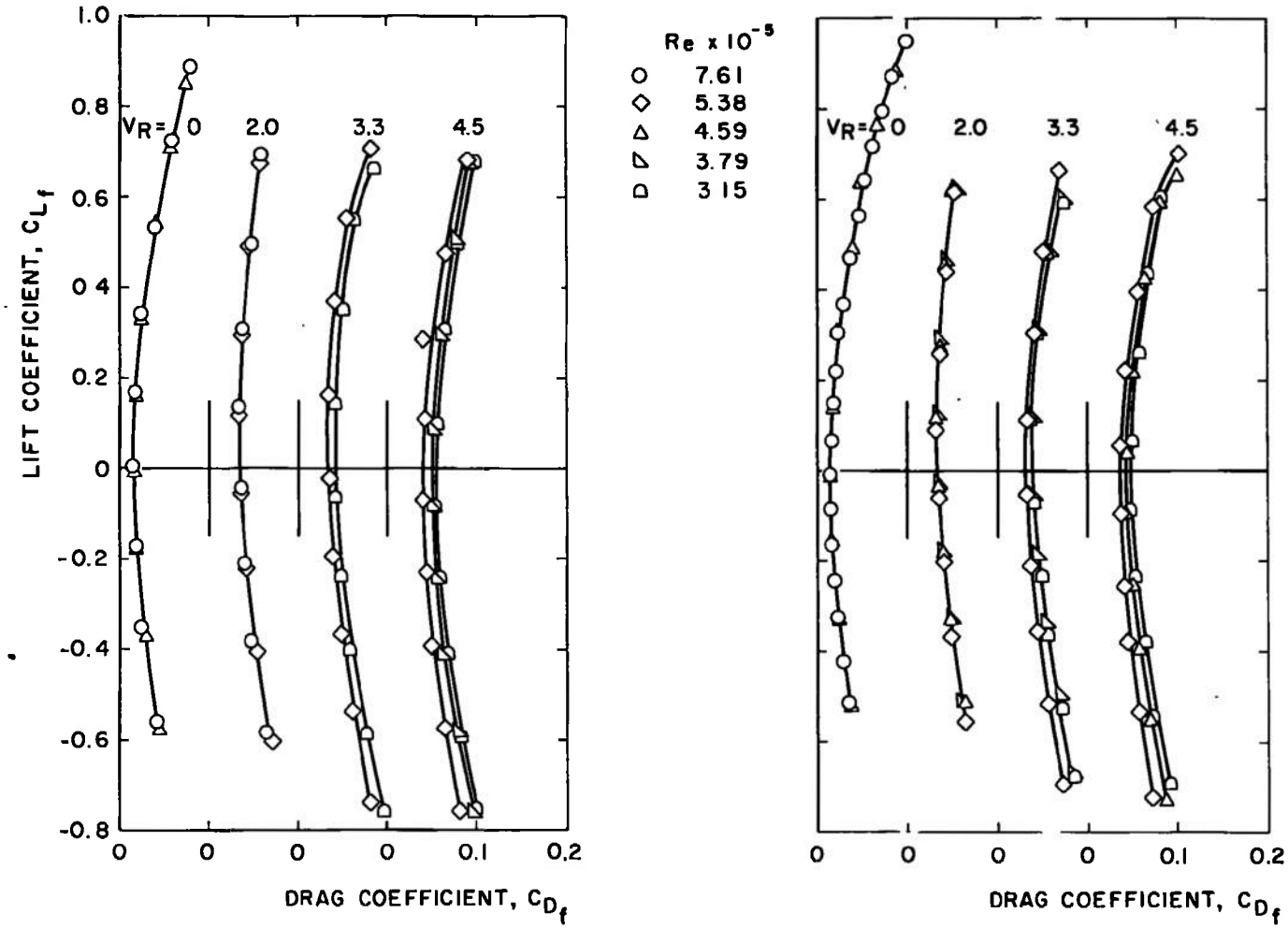

a. Tail-On

b. Tail-Off

Fig. 7 Interference-Free Drag Coefficient

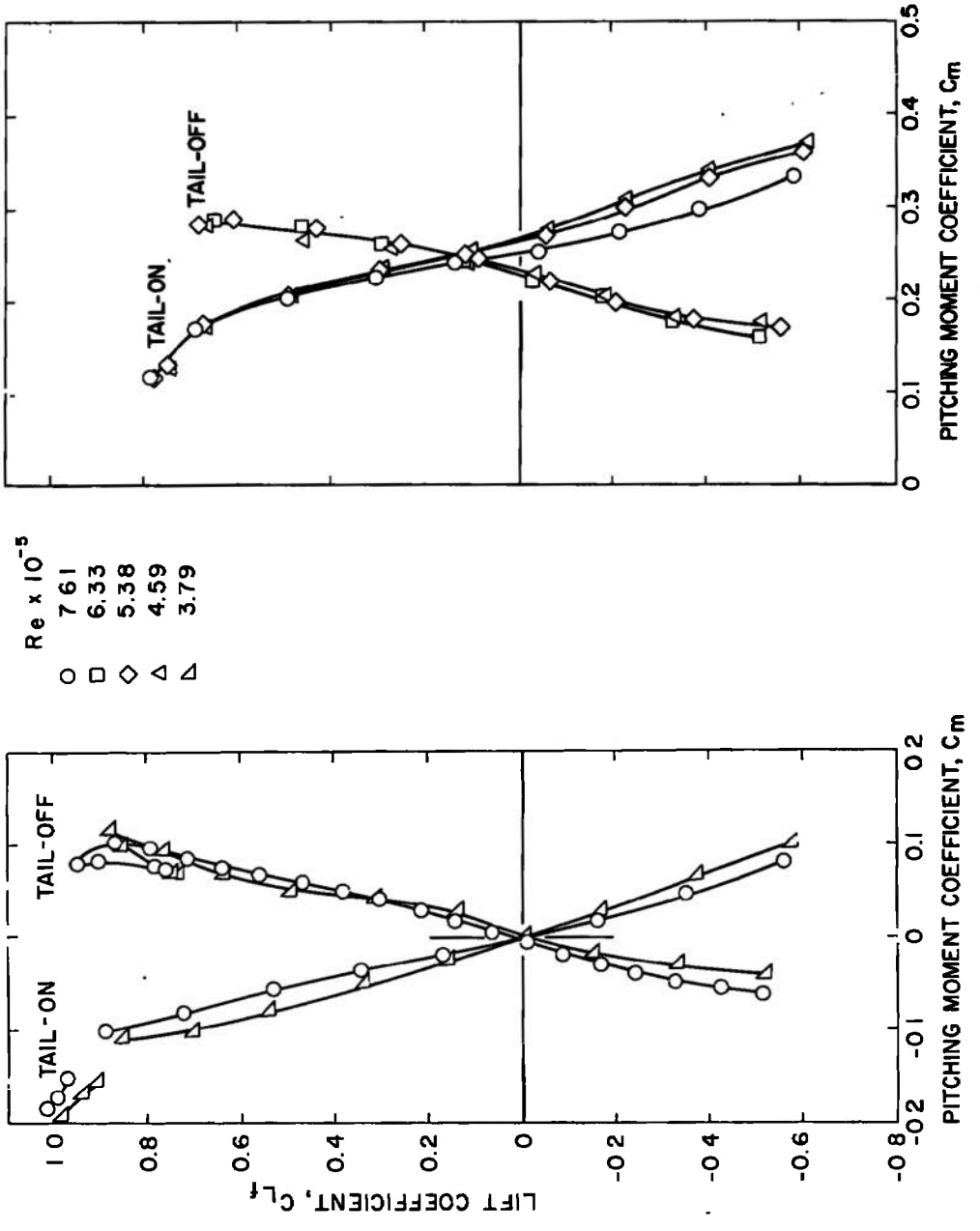

Fig. 8 Interference-Free Pitching Moment Coefficient

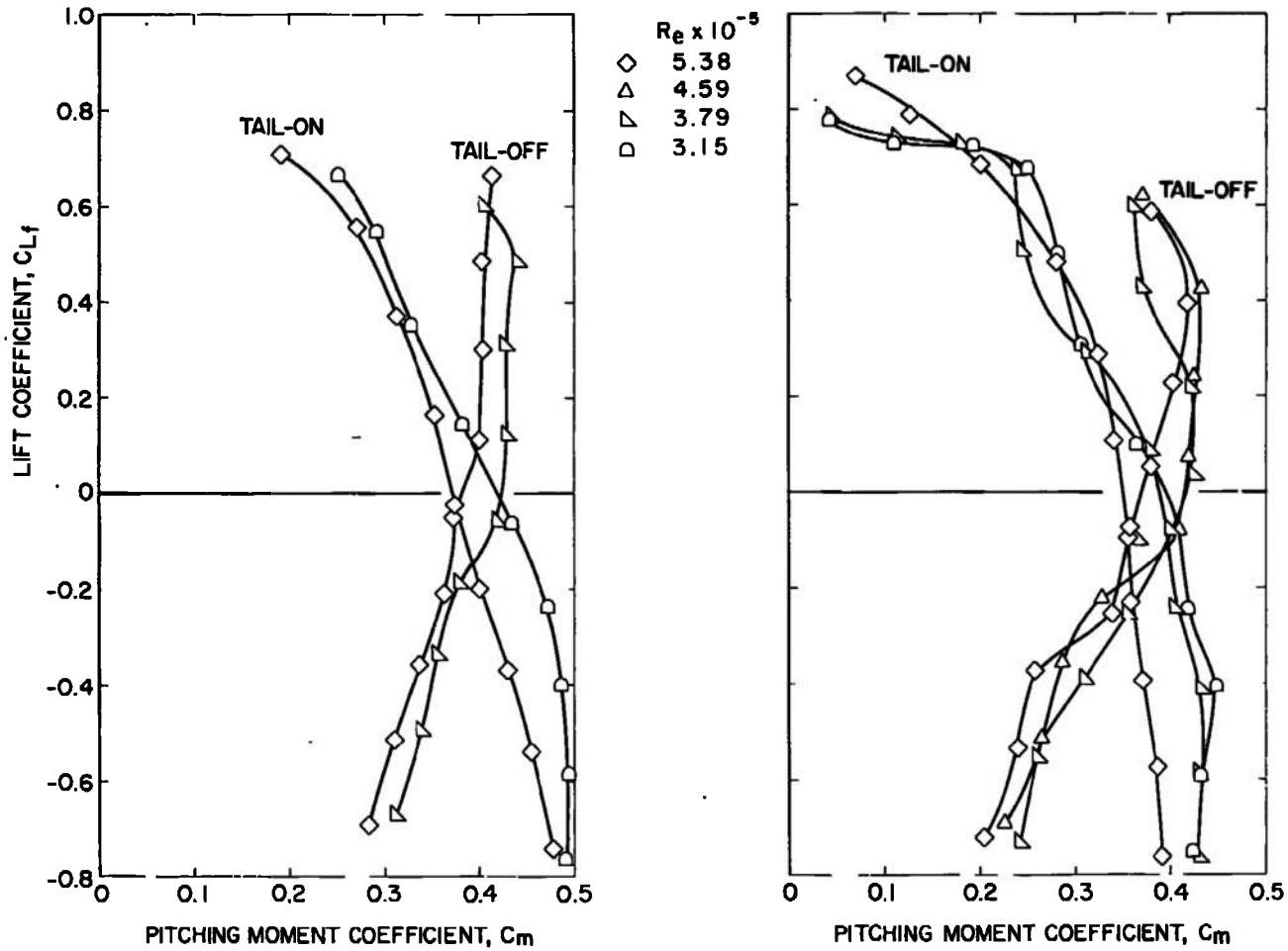

c. V_R = 3.3

d. V_R = 4.5

Fig. 8 Concluded

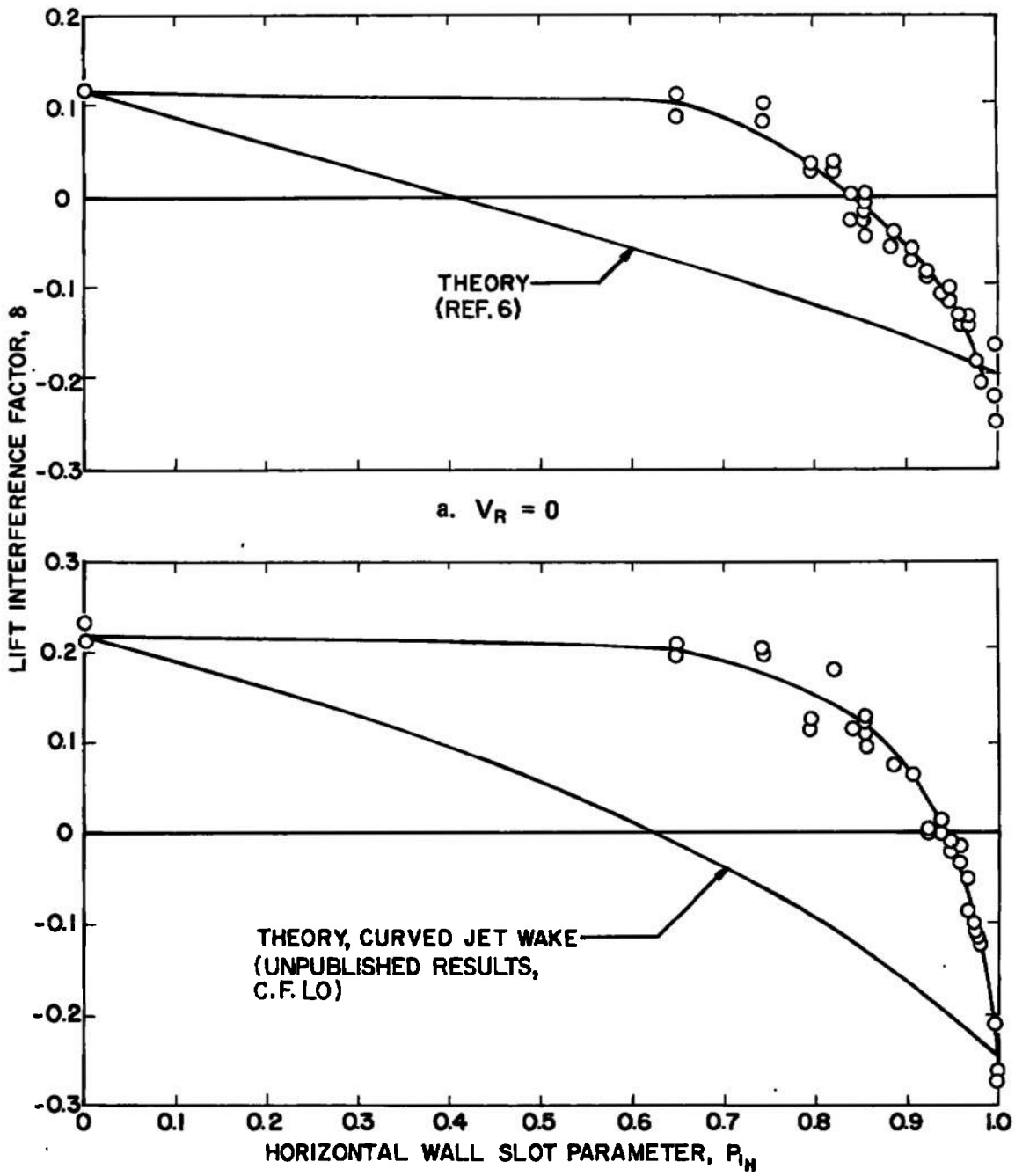

Fig. 9 Lift Interference Factor versus Slot Parameter P_1, Configuration A

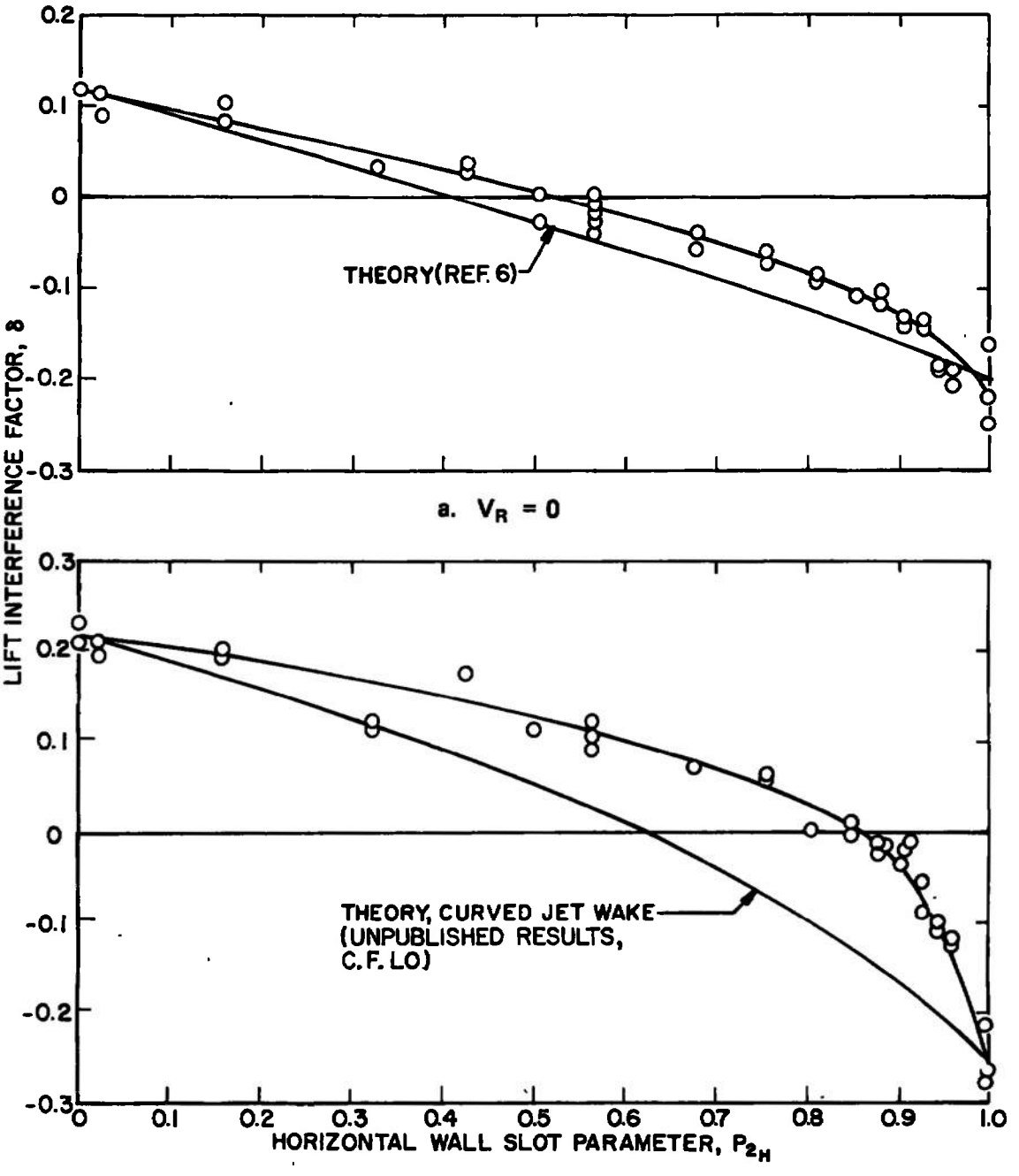

Fig. 10 Lift Interference Factor versus Slot Parameter P_2, Configuration A

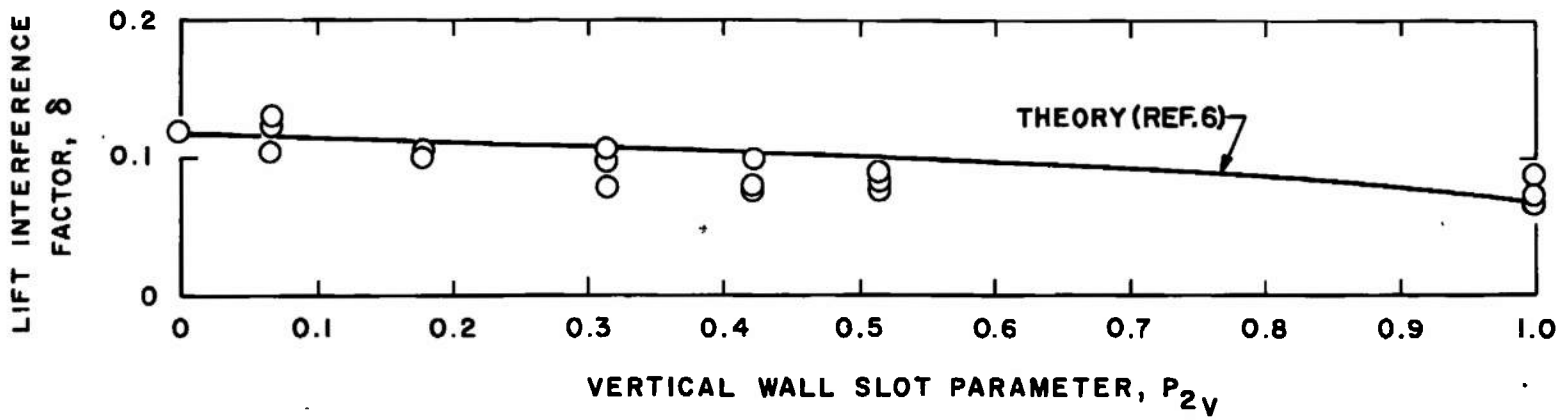

Fig. 11 Effect of Slots in Vertical Wall, Slot Configuration A, Solid Horizontal Walls, $V_R = 0$

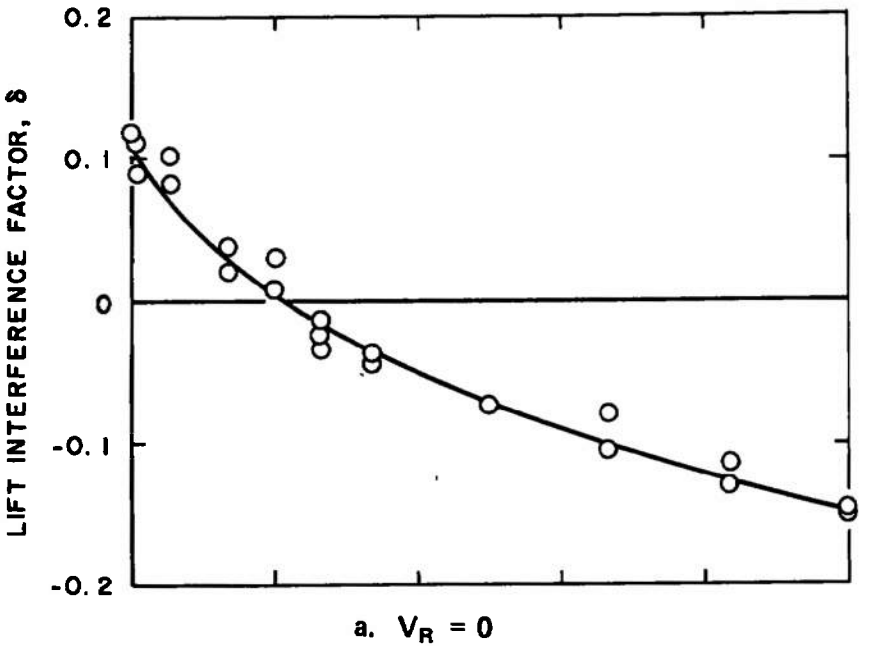

a. $V_R = 0$

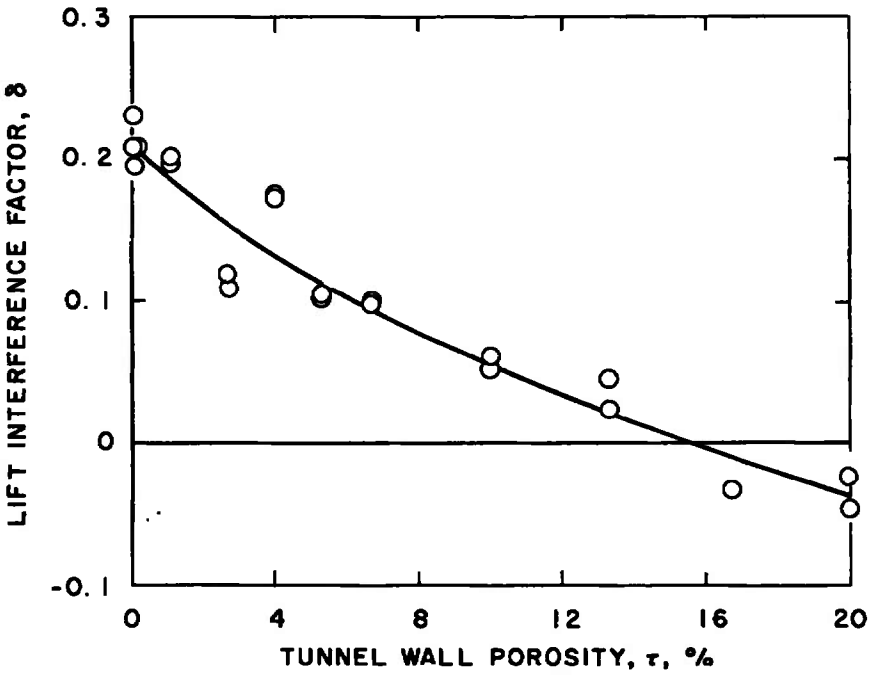

b. $V_R = 4.5$

Fig. 12 Lift Interference Factor versus Porosity, Configuration A

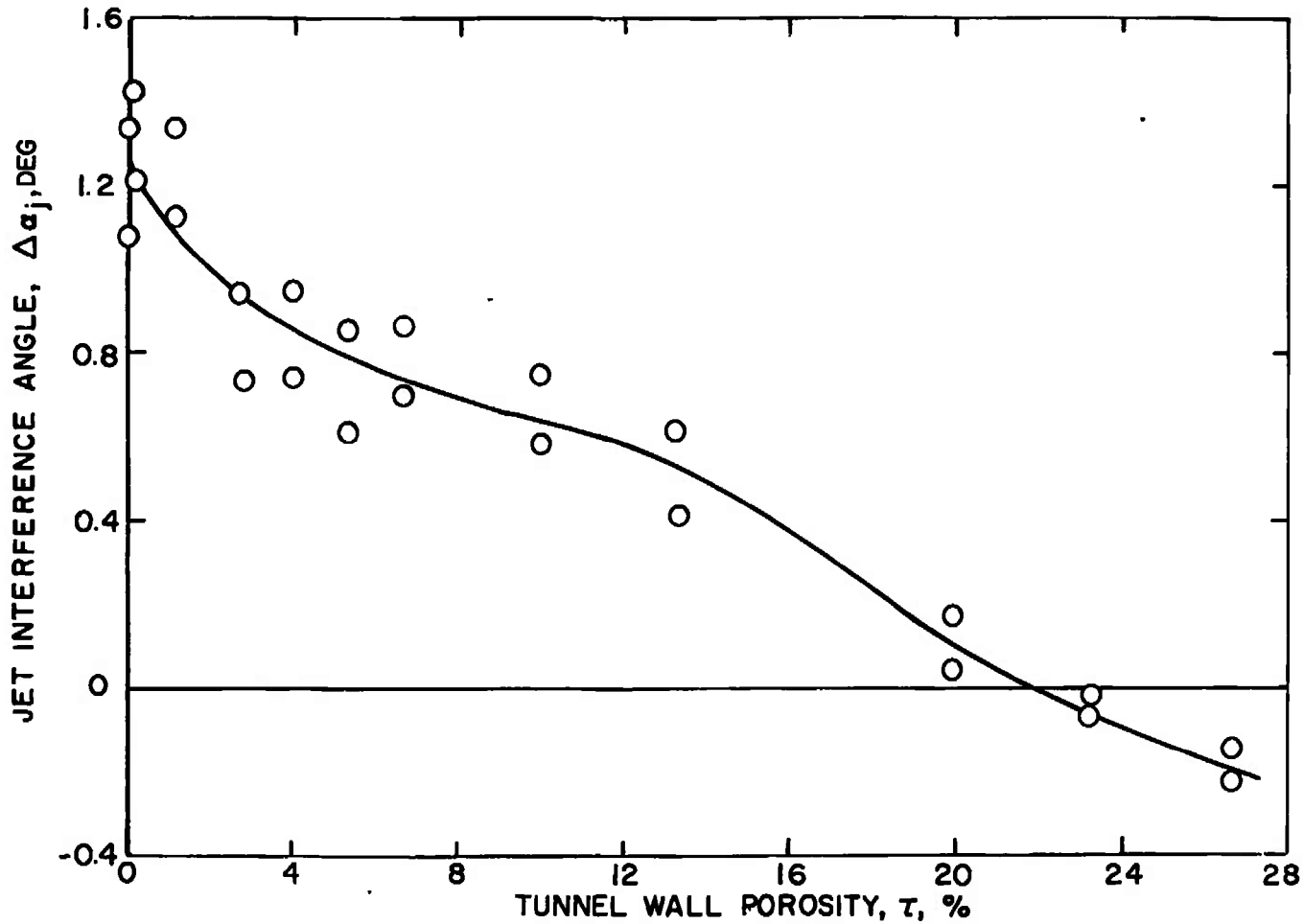

Fig. 13 Jet Interference Angle versus Porosity, Configuration A, V_R = 4.5

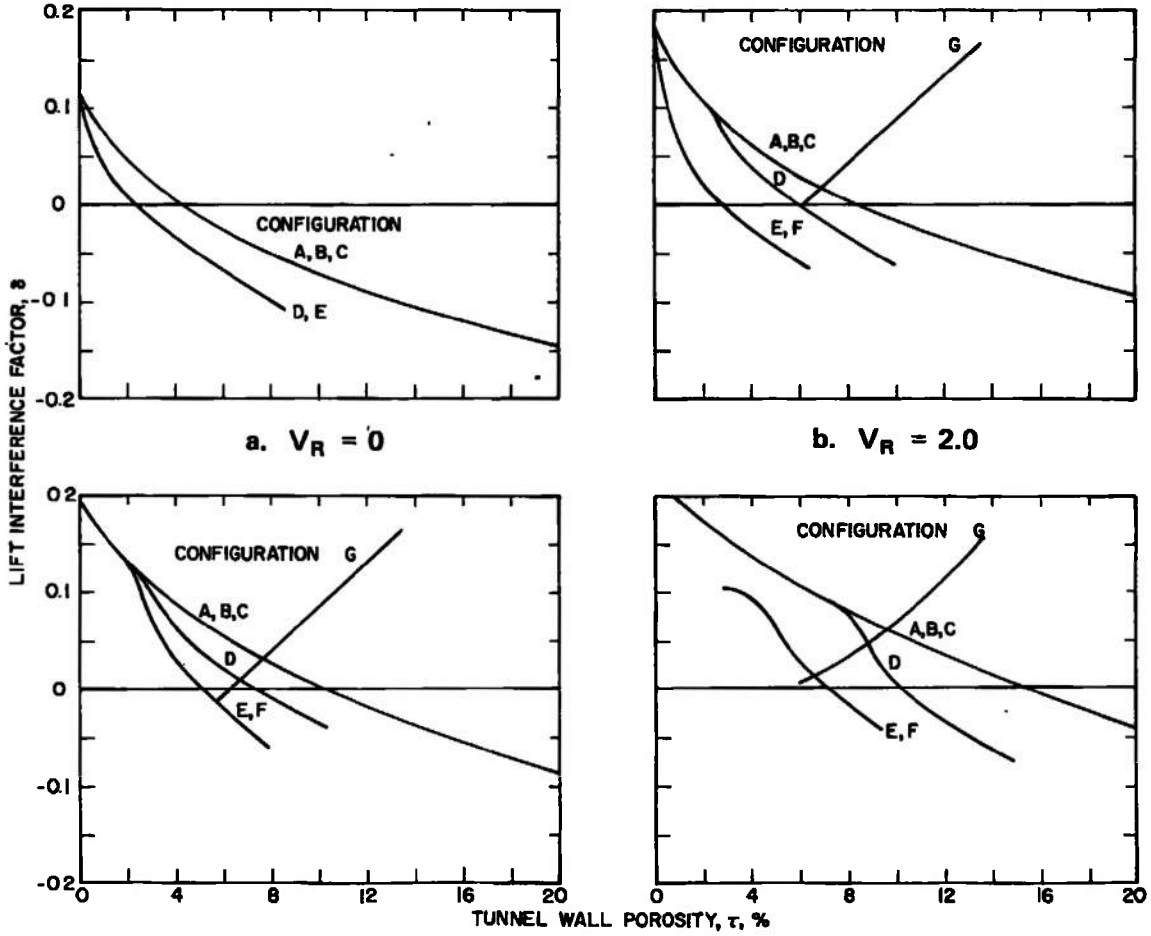

Fig. 14 Effect of Wall Configuration on the Lift Interference Factor

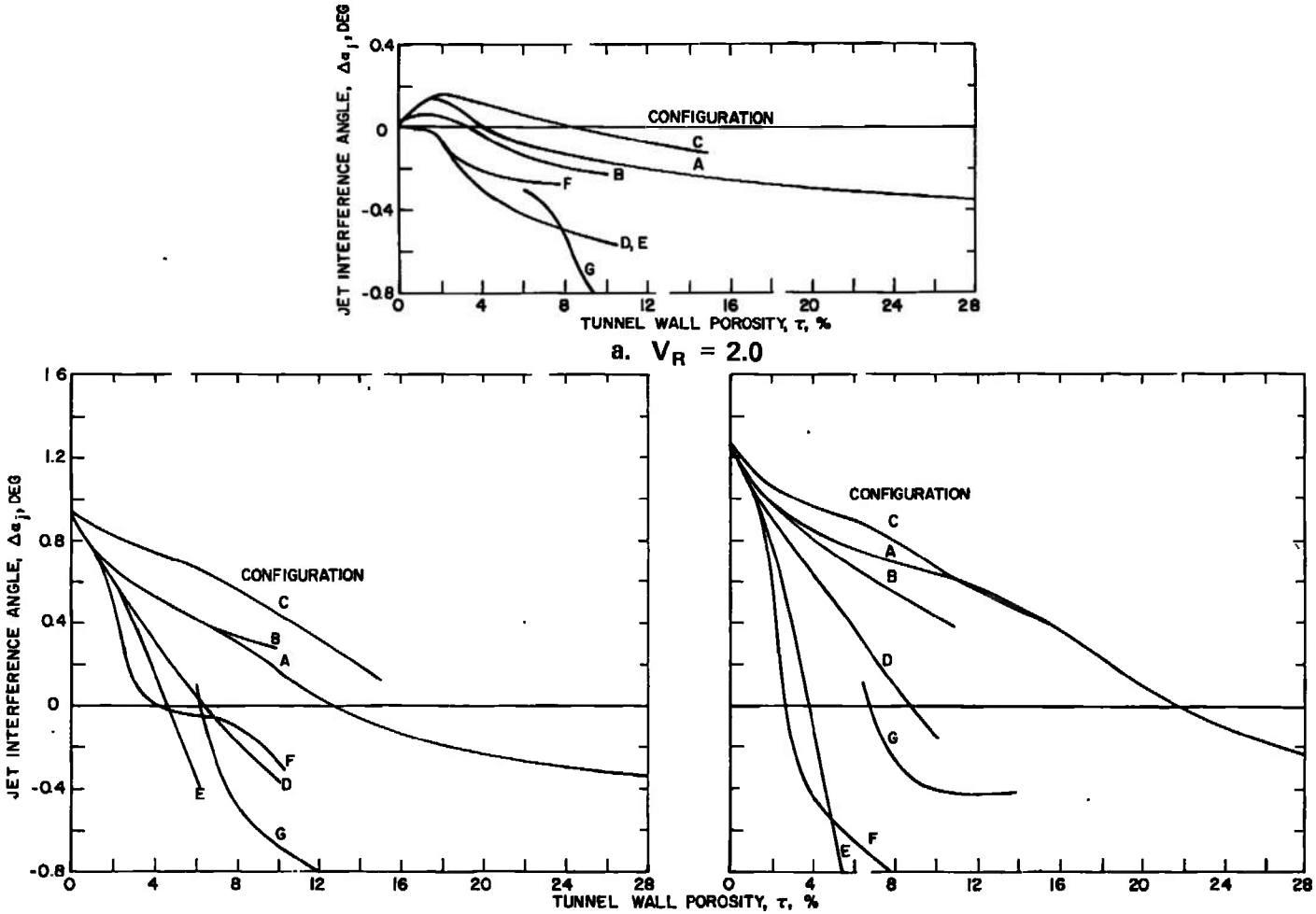

Fig. 15 Effect of Wall Configuration on the Jet Interference Angle

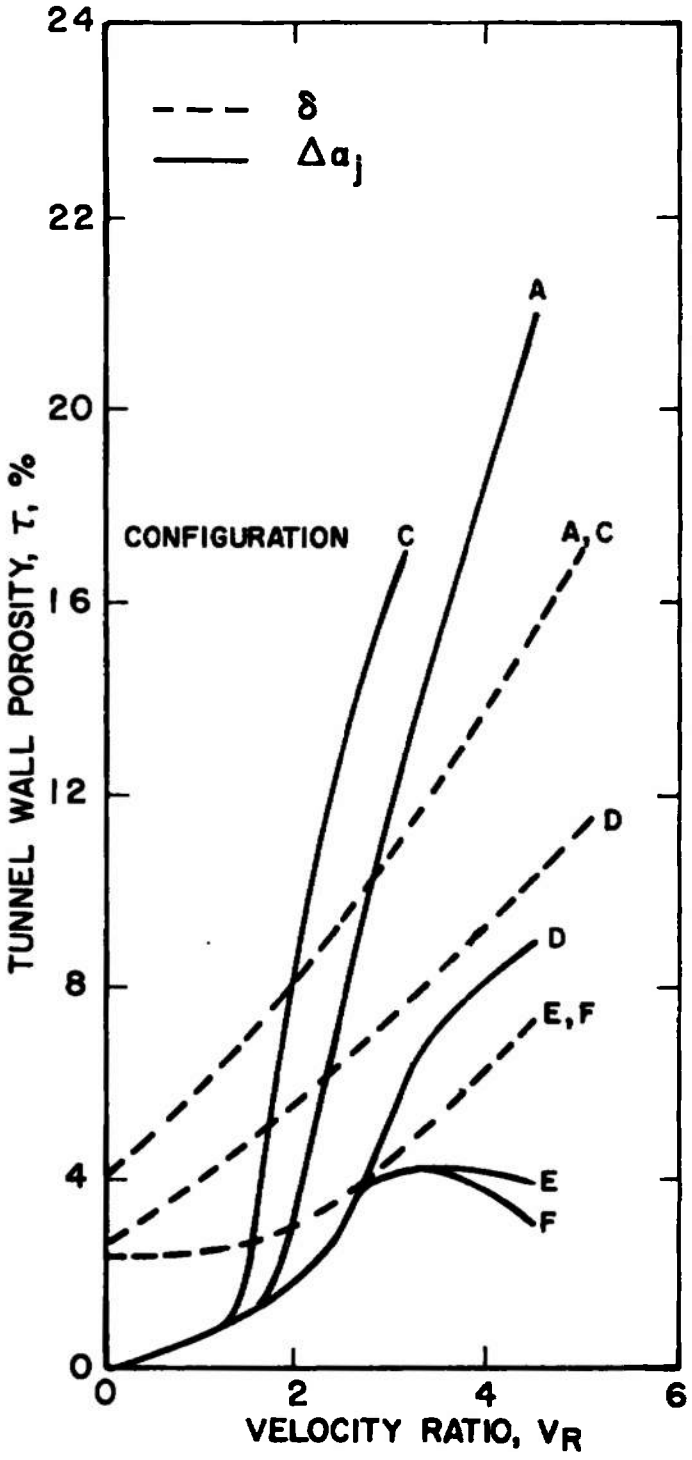

Fig. 16 Porosity Required for Zero δ and Δa_j

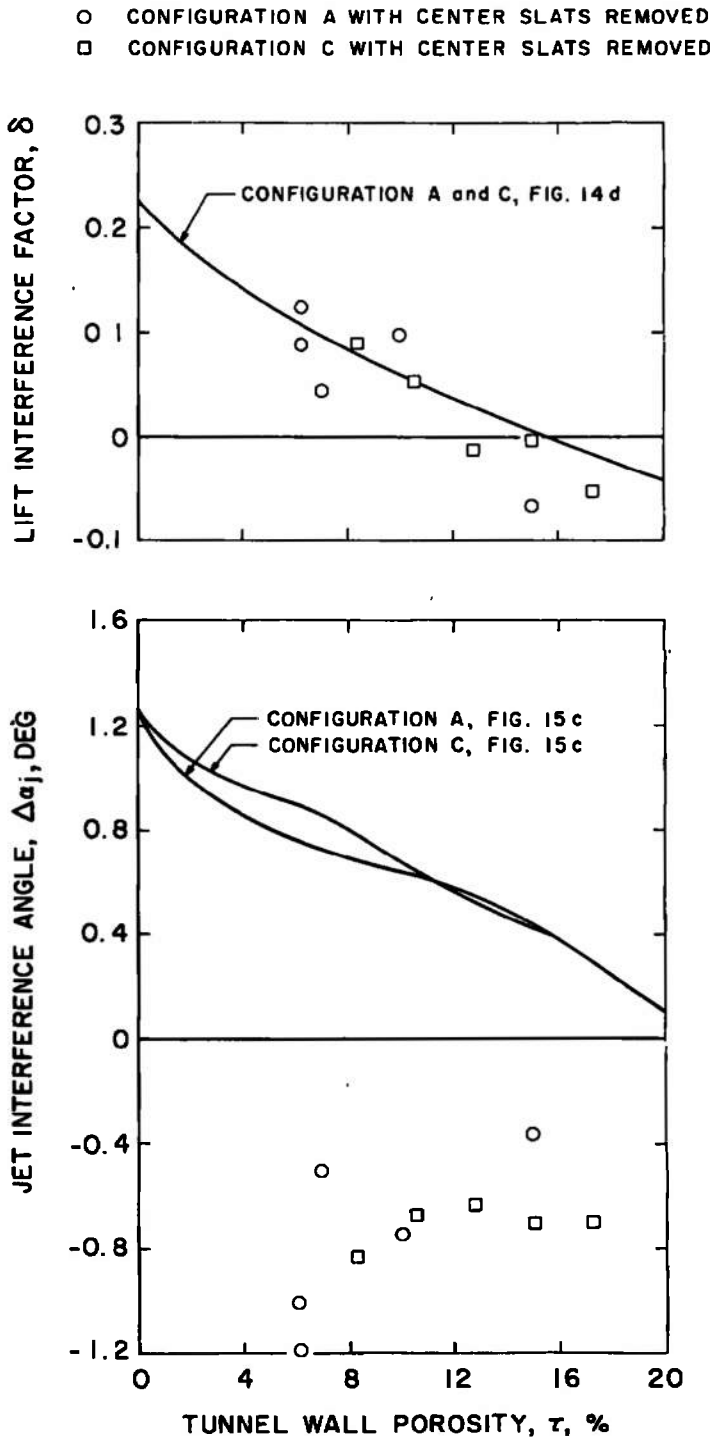

Fig. 17 The Effect of Removing the Center Slat on δ and $\Delta\alpha_j$, Configuration A, V_R = 4.5

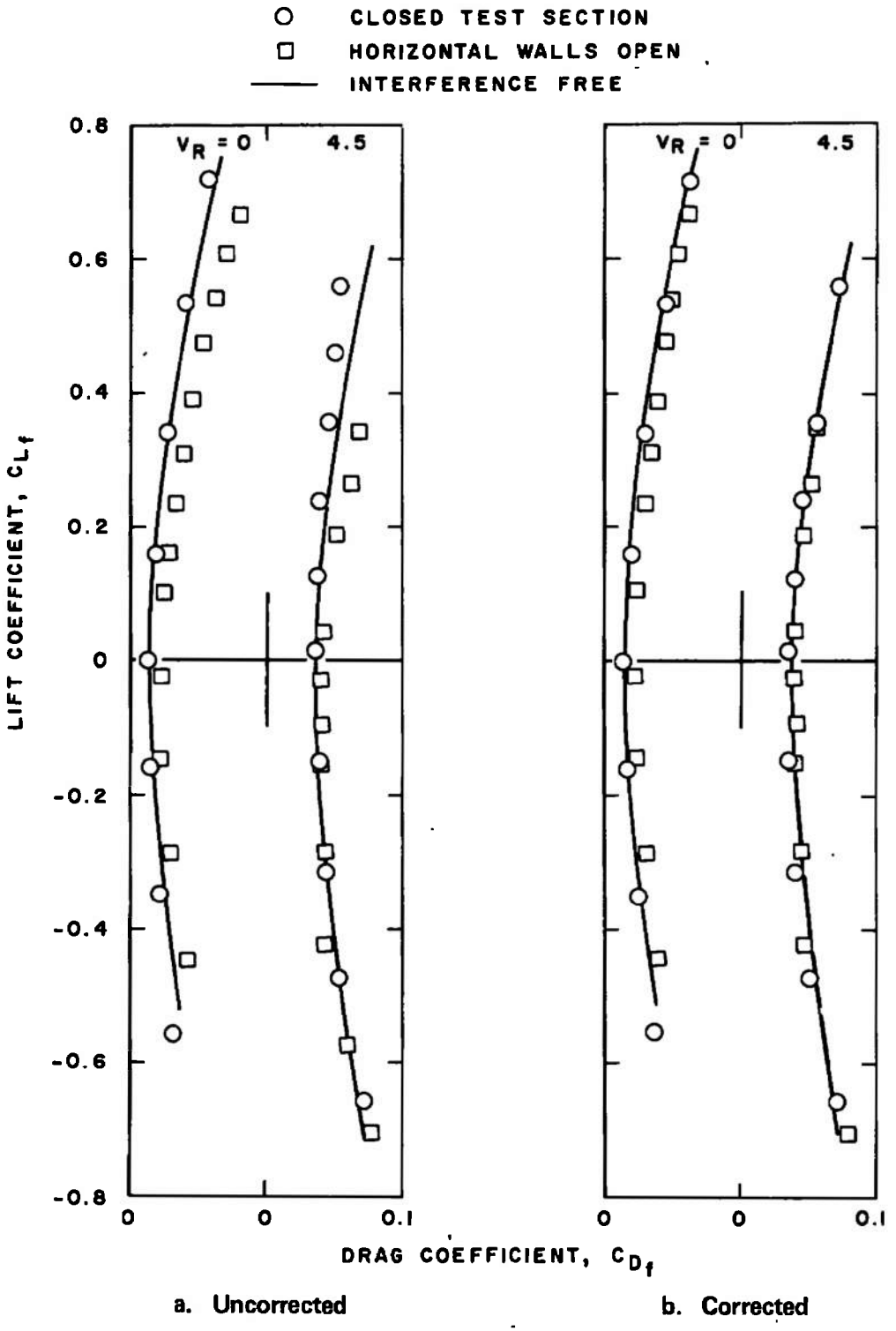

a. Uncorrected b. Corrected

Fig. 18 Effect of Open and Closed Walls on Drag Coefficient

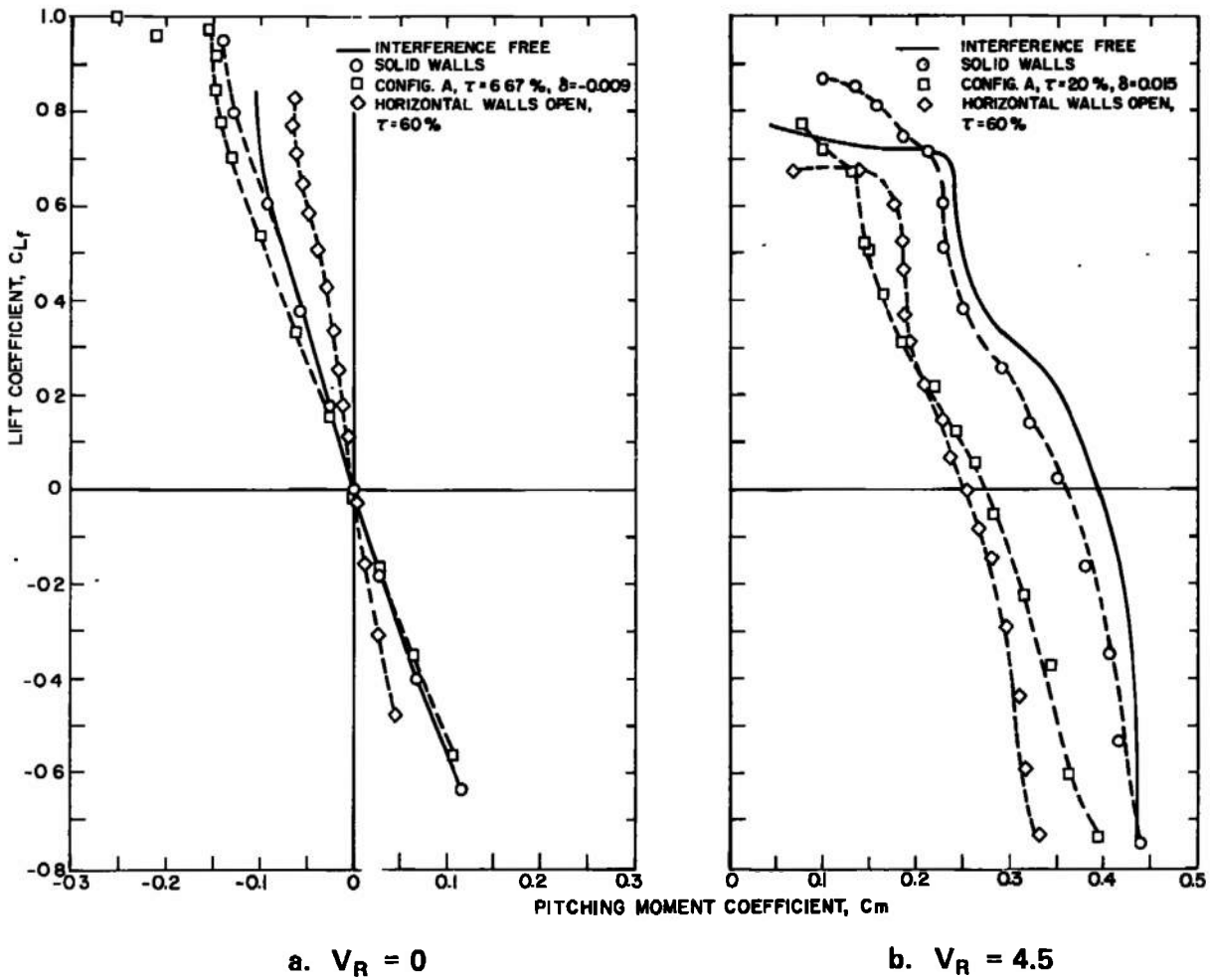

a. $V_R = 0$ b. $V_R = 4.5$

Fig. 19 Comparison of Pitching Moment for Closed Walls, Open Horizontal Walls, and Configuration A. with $\delta \approx 0$, Tail-On

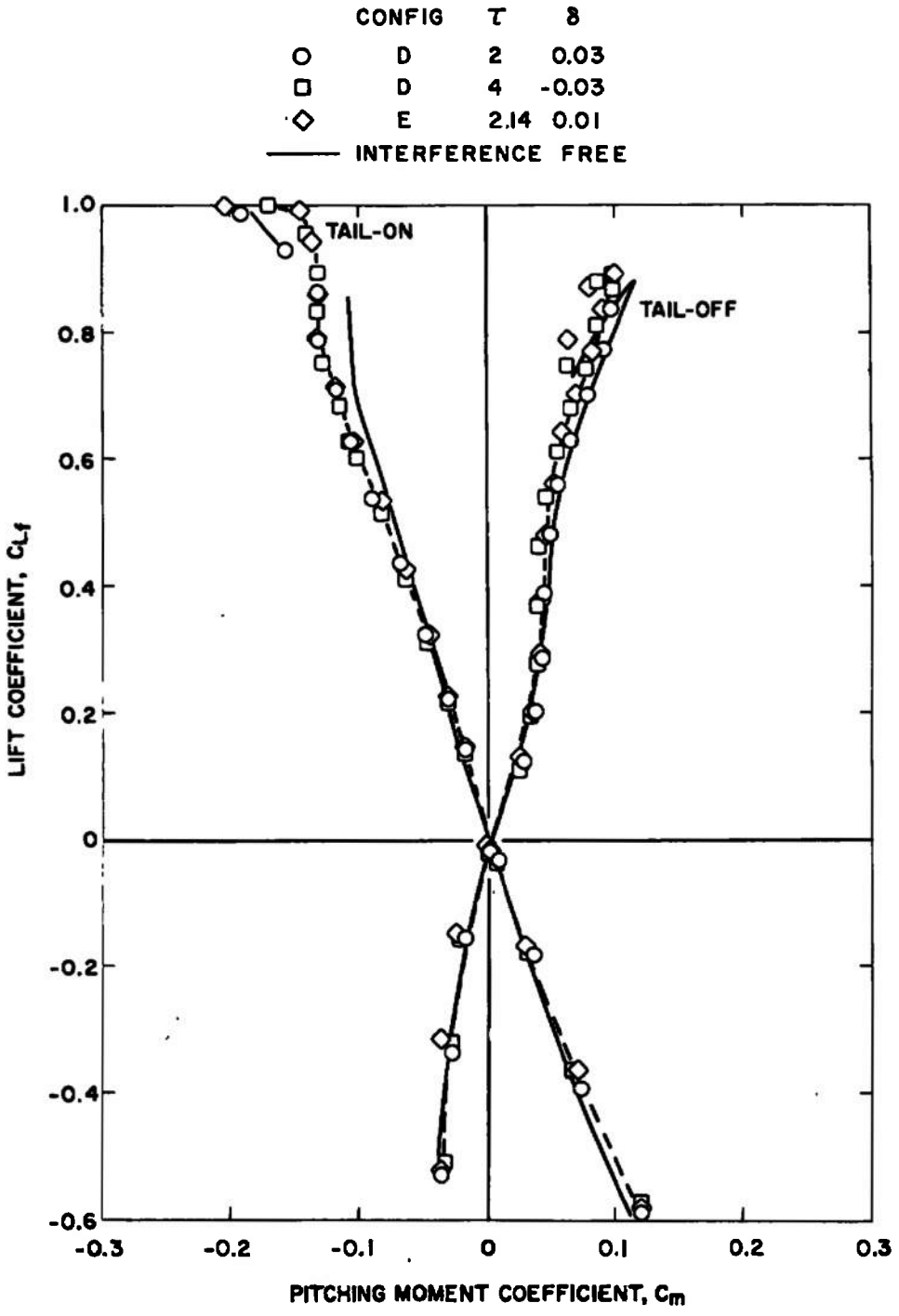

Fig. 20 Pitching Moment for Configurations D and E with $\delta \approx 0$, $V_R = 0$

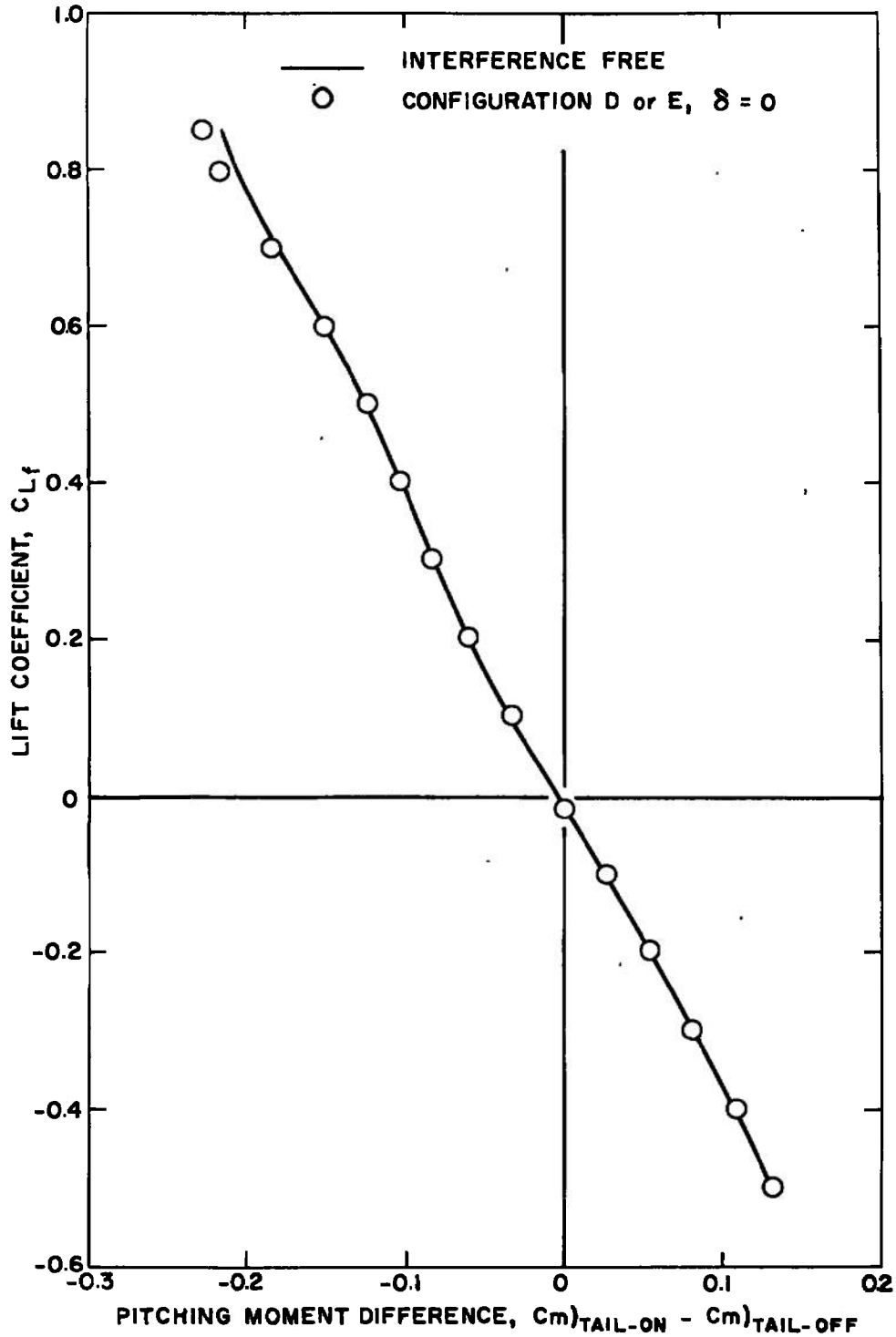

Fig. 21 Difference between Tail-On and Tail-Off Pitching Moment, Configurations D and E, $\delta \approx 0$, $V_R = 0$

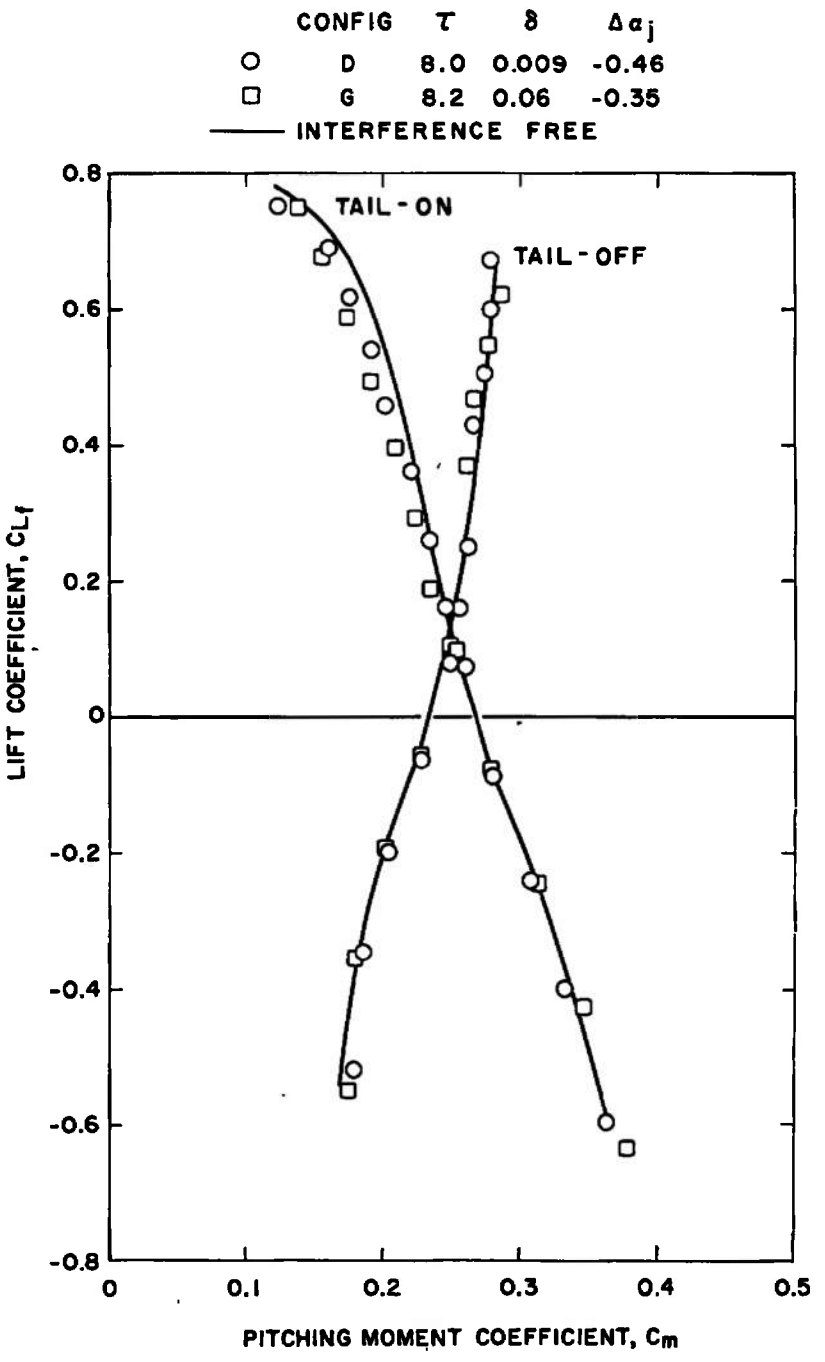

Fig. 22 Pitching Moment with Configuration D, τ = 8 percent, and Configuration G, τ = 8.2 percent, V_R = 2.0

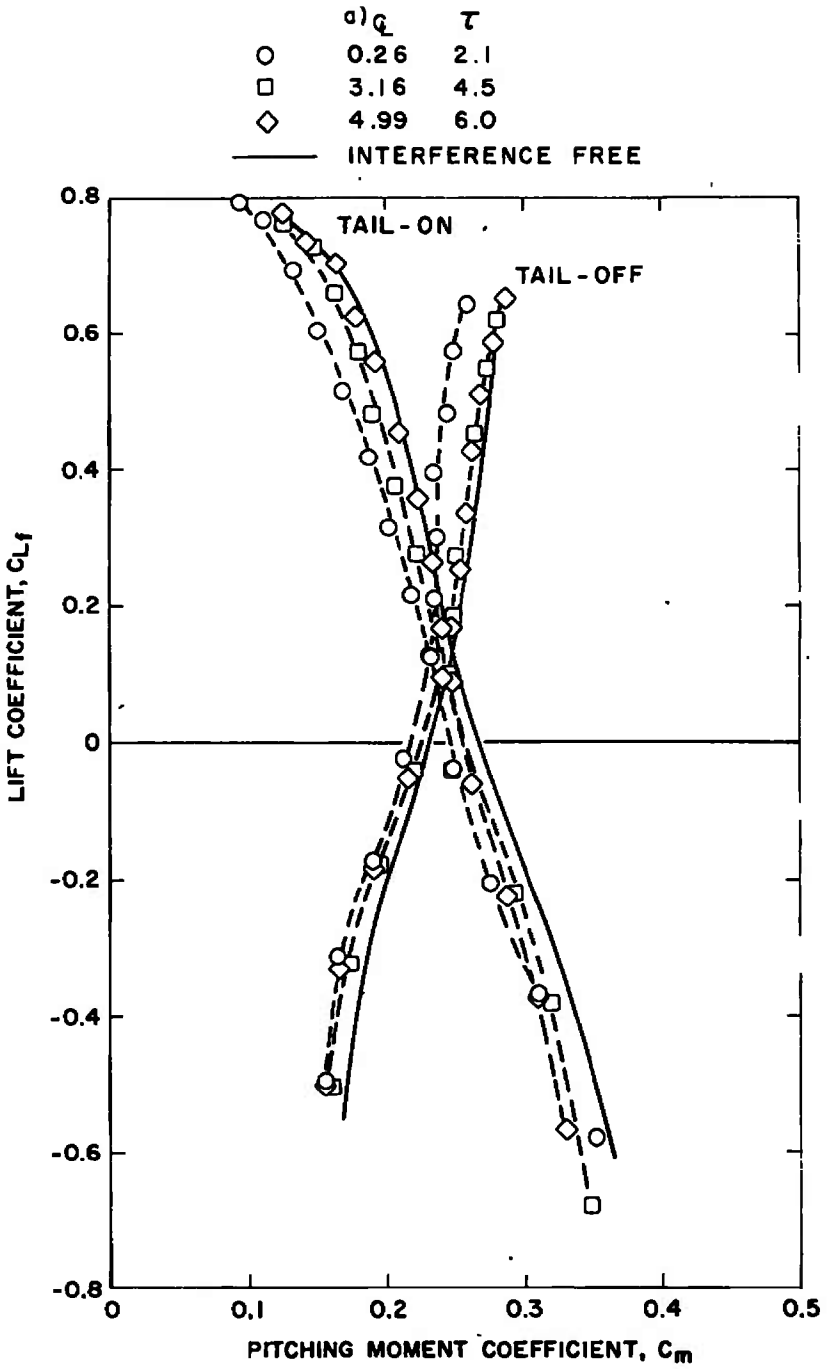

Fig. 23 Effect of Varying the Center Slot Width on Pitching Moment, Configuration E, V_R = 2.0

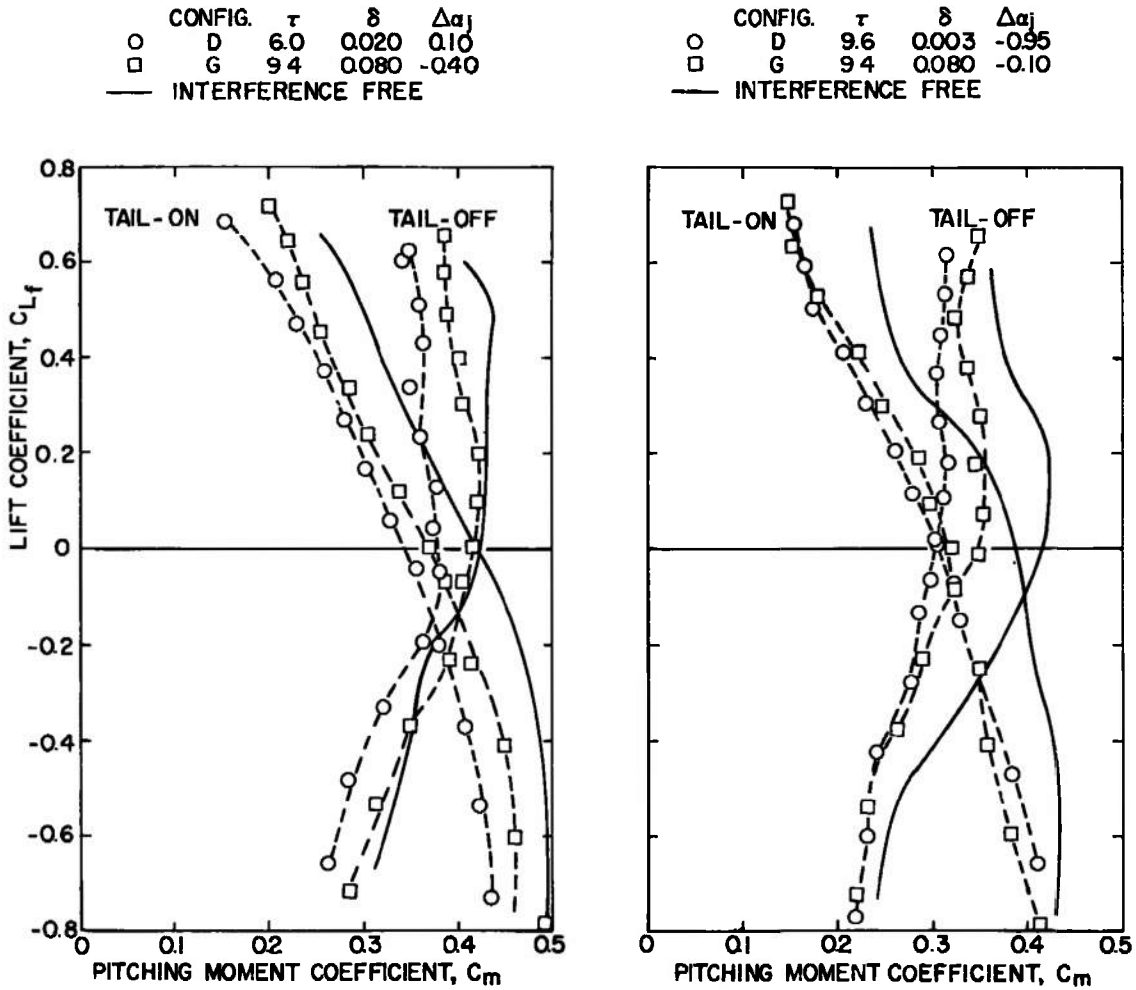

a. $V_R = 3.3$ b. $V_R = 4.5$

Fig. 24 Pitching Moment with Configuration D, $\delta \approx 0$, and Configuration G, $\tau = 9.4$ percent

APPENDIX II
EXPERIMENTAL INCIDENT CORRECTION FACTORS

The equivalent free-air angle of attack of a V/STOL model in the wind tunnel is given by

$$\alpha = \alpha_m + \delta \frac{S}{C} C_L + \Delta\alpha_j \qquad \text{(II-1)}$$

A relation relating the free-air angle of attack to the lift coefficient,

$$\alpha = f(C_L) = a_0 - a_1 C_L + a_2 C_L{}^2 - a_3 C_L{}^3 + \cdots \qquad \text{(II-2)}$$

was obtained by a least-squares curve fit of the LTV data for a given velocity ratio and model configuration. Each data point from the V/STOL tunnel yielded a pair of values for the lift coefficient and angle of attack (α_{m_i}, C_{L_i}). The error associated with each pair of values, obtained by subtracting Eqs. (II-1) and (II-2), is

$$E_i = \alpha_{m_i} + \delta \frac{S}{C} C_{L_i} + \Delta\alpha_j - f(C_{L_i})$$

It is desired to minimize the error for a set of data by selecting appropriate values of the constants δ and $\Delta\alpha_j$ in the least-squares sense. The sum of the squares of the error is given by

$$\sum_1^N E_i^2 = \sum_1^N [\alpha_i + \delta \frac{S}{C} C_{L_i} + \Delta\alpha_j - f(C_{L_i})]^2 \qquad \text{(II-3)}$$

where N is the number of data points in a given set of data. A set is comprised of all (α_{m_i}, C_{L_i}) points obtained with a given model configuration (tail-on or tail-off), tunnel wall configuration and velocity ratio between an angle of attack of -6 deg and the model stall point which was, in general, near 9 deg.

The minimum value for Eq. (II-3) is obtained when

$$\frac{\partial}{\partial\delta} \sum_1^N E_i^2 = 0 = 2 \sum_1^N [\alpha_i + \delta \frac{S}{C} C_{L_i} + \Delta\alpha_j - f(C_{L_i})] \frac{S}{C} C_{L_i}$$

and

$$\frac{\partial}{\partial\Delta\alpha_j} \sum_1^N E_i^2 = 0 = 2 \sum_1^N [\alpha_i + \delta \frac{S}{C} C_{L_i} + \Delta\alpha_j - f(C_{L_i})]$$

which may be rewritten as

$$\delta \frac{S}{C} \sum_{1}^{N} C_{L_i}{}^2 + \Delta\alpha_j \sum_{1}^{N} C_{L_i} = \sum_{1}^{N} [f(C_{L_i}) - \alpha_i] C_{L_i} \tag{II-4}$$

and

$$\delta \frac{S}{C} \sum_{1}^{N} C_{L_i} + \Delta\alpha_j N = \sum_{1}^{N} [f(C_{L_i}) - \alpha_i] \tag{II-5}$$

The desired quantities are obtained by the simultaneous solution of Eqs. (II-4) and (II-5) which give

$$\delta = \frac{C}{S} \frac{N \sum_{1}^{N} [f(C_{L_i}) - \alpha_i] C_{L_i} - \sum_{1}^{N} [f(C_{L_i}) - \alpha_i] \sum_{1}^{N} C_{L_i}}{N \sum_{1}^{N} C_{L_i}{}^2 - (\sum_{1}^{N} C_{L_i})^2} \tag{II-6}$$

and

$$\Delta\alpha_j = \frac{\sum_{1}^{N} [f(C_{L_i}) - \alpha_i] \sum_{1}^{N} C_{L_i}{}^2 - \sum_{1}^{N} [f(C_{L_i}) - \alpha_i] C_{L_i} \sum_{1}^{N} C_{L_i}}{N \sum_{1}^{N} C_{L_i}{}^2 - (\sum_{1}^{N} C_{L_i})^2} \tag{II-7}$$

UNCLASSIFIED

Security Classification

DOCUMENT CONTROL DATA - R & D

(Security classification of title, body of abstract and indexing annotation must be entered when the overall report is classified)

1. ORIGINATING ACTIVITY *(Corporate author)*
Arnold Engineering Development Center,
ARO, Inc., Operating Contractor,
Arnold Air Force Station, Tennessee 37389

2a. REPORT SECURITY CLASSIFICATION
UNCLASSIFIED

2b. GROUP
N/A

3 REPORT TITLE
AN INVESTIGATION OF SEVERAL SLOTTED WIND TUNNEL WALL CONFIGURATIONS WITH A HIGH DISC LOADING V/STOL MODEL

4. DESCRIPTIVE NOTES *(Type of report and inclusive dates)*
July 1, 1966 to June 30, 1970--Final Report

5. AUTHOR(S) *(First name, middle initial, last name)*
T. W. Binion, Jr., ARO, Inc.

6. REPORT DATE	7a. TOTAL NO. OF PAGES	7b. NO. OF REFS
May 1971	64	26

8a. CONTRACT OR GRANT NO.	9a. ORIGINATOR'S REPORT NUMBER(S)
F40600-71-C-0002	
b. PROJECT NO. Program Element 64719F	AEDC-TR-71-77
c.	9b. OTHER REPORT NO(S) *(Any other numbers that may be assigned this report)* ARO-PWT-TR-71-43
d.	

10 DISTRIBUTION STATEMENT
Approved for public release; distribution unlimited.

11. SUPPLEMENTARY NOTES	12. SPONSORING MILITARY ACTIVITY
Available in DDC	Arnold Engineering Development Center, Air Force Systems Command, Arnold AF Station, Tennessee 37389

13. ABSTRACT

With the advent of V/STOL model configurations, it bacame apparent that classical solutions to wind tunnel wall interference problems were not adequate to produce interference-free test results with augmented lift models. The investigation reported herein is the experimental portion of a unified theoretical and experimental search for a slotted wind tunnel wall configuration with minimal interference for conventional and V/STOL models. It is shown that theory and experiment are in excellent agreement for the classical case provided an appropriate expression is used to relate the wall geometry to the boundary condition. Classical data correction equations are not appropriate for the V/STOL case, however. An additional term, not predicted by theory, is needed to account for changes in the jet wake. Geometric parameters which influence the wall interference quantities are indicated. Wall configurations are shown which will produce interference-free force data to a jet-to-free-stream velocity ratio of 4.5. However, additional development work is needed to simultaneously obtain interference-free pitching moment data at velocity ratios greater than two.

DD FORM 1 NOV 65 1473

UNCLASSIFIED

Security Classification

14. KEY WORDS	LINK A		LINK B		LINK C	
	ROLE	WT	ROLE	WT	ROLE	WT
vertical takeoff aircraft						
short takeoff aircraft						
scale models						
test facilities						
wind tunnels						
slots						
porosity						

AFSC
Arnold AFS Tenn